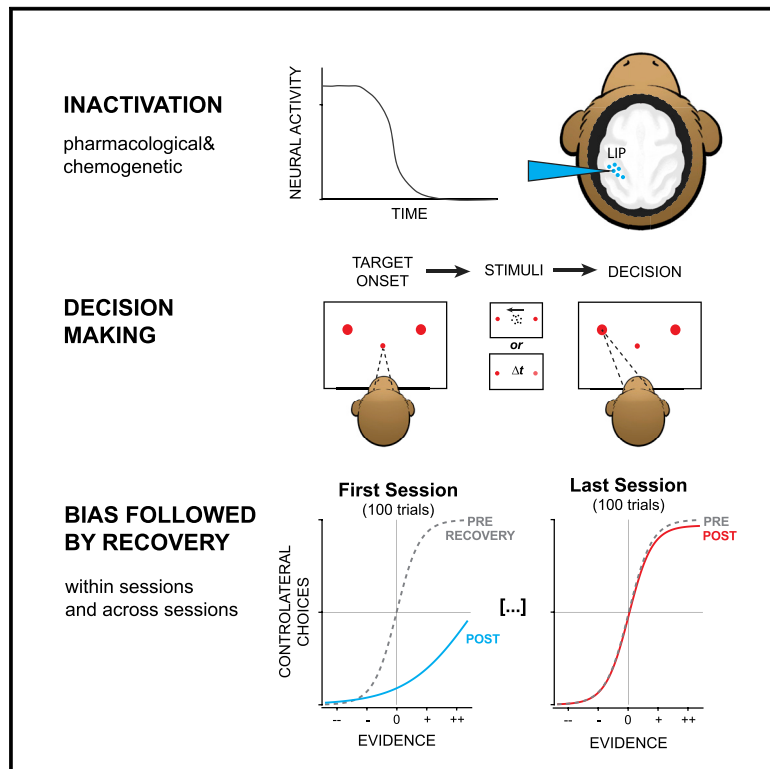


# Deficits in decision-making induced by parietal cortex inactivation are compensated at two timescales

## Graphical abstract



## Authors

Danique Jeurissen, S. Shushruth, Yasmine El-Shamayleh, Gregory D. Horwitz, Michael N. Shadlen

## Correspondence

d.jeurissen@columbia.edu (D.J.), shushruth@gmail.com (S.S.), shadlen@columbia.edu (M.N.S.)

## In brief

Jeurissen et al. inactivate a parietal cortical area thought to play a role in perceptual decision-making. Silencing causes monkeys to bias decisions, consistent with partial hemineglect. The bias dissipates over 30 min and over subsequent experiments. The results expose a capacity of the brain to compensate for focal insult.

## Highlights

- Unilateral inactivation of area LIP biases perceptual decisions, but only transiently
- The bias dissipates rapidly despite silencing and decreases in subsequent sessions
- Compensation by unaffected circuits may explain weak or null effects of inactivation



Report

# Deficits in decision-making induced by parietal cortex inactivation are compensated at two timescales

Danique Jeurissen,<sup>1,2,5,\*</sup> S. Shushruth,<sup>1,5,\*</sup> Yasmine El-Shamayleh,<sup>1</sup> Gregory D. Horwitz,<sup>4</sup> and Michael N. Shadlen<sup>1,2,3,6,\*</sup>

<sup>1</sup>Zuckerman Mind Brain Behavior Institute, Department of Neuroscience, Columbia University, New York, NY 10027, USA

<sup>2</sup>Howard Hughes Medical Institute, Columbia University, New York, NY 10027, USA

<sup>3</sup>Kavli Institute, Columbia University, New York, NY 10027, USA

<sup>4</sup>Department of Physiology & Biophysics, Washington National Primate Research Center, University of Washington, Seattle, WA 98195, USA

<sup>5</sup>These authors contributed equally

<sup>6</sup>Lead contact

\*Correspondence: [d.jeurissen@columbia.edu](mailto:d.jeurissen@columbia.edu) (D.J.), [shushruth@gmail.com](mailto:shushruth@gmail.com) (S.S.), [shadlen@columbia.edu](mailto:shadlen@columbia.edu) (M.N.S.)

<https://doi.org/10.1016/j.neuron.2022.03.022>

## SUMMARY

Perceptual decisions arise through the transformation of samples of evidence into a commitment to a proposition or plan of action. Such transformation is thought to involve cortical circuits capable of computation over timescales associated with working memory, attention, and planning. Neurons in the lateral intraparietal area (LIP) play a role in these functions, and much of what is known about the neurobiology of decision-making has been influenced by studies of LIP and its network of connections. However, the causal role of LIP remains controversial. In this study, we used pharmacological and chemogenetic methods to inactivate LIP in one brain hemisphere of four rhesus monkeys. This inactivation produced biases in decisions, but the effects dissipated despite persistent neural inactivation, implying compensation by unaffected areas. Compensation occurred rapidly within an experimental session and more gradually across sessions. These findings resolve disparate studies and inform the interpretation of focal perturbations of brain function.

## INTRODUCTION

A decision is a commitment to a proposition or plan of action based on evidence from the environment or memory. The process involves a network of brain areas spanning the association areas of the cerebral cortex as well as their subcortical connections. Even a simple decision to look to the left or right, based on visual evidence from straight ahead, is known to involve neurons in the dorsolateral prefrontal cortex, frontal eye field, striatum, superior colliculus, and lateral intraparietal (LIP) area (Shadlen and Newsome, 1996; Kim and Shadlen, 1999; Horwitz et al., 2004; Ding and Gold, 2010, 2012). Neurons in these areas represent both the saccadic choice and the evolving deliberative process—the integration of noisy evidence leading to the choice (Shadlen and Kiani, 2013).

The evidence accumulation process has been characterized extensively in area LIP. Neurons in LIP combine accumulating evidence with other factors, including biases (e.g., prior probability) and time costs to establish a representation (the decision variable) suitable for terminating the process. However, whether LIP, or any other single area, is essential to this process remains unclear. Causal perturbations of LIP activity have led to mixed results. Hanks et al. (2006) showed that electrical microstimulation

of neurons that represent one of two choice targets caused a small bias in favor of that choice. The bias was associated with changes in response time by an amount consistent with a change in the firing rates of neurons that represent the decision variable. However, inactivation of LIP has not produced consistent effects on choice. Chen et al. (2020) observed striking biases against choice targets in the visual hemifield contralateral to cryo-inactivated posterior parietal cortex, including area LIP. Yet, two recent studies used intraparenchymal infusions of the GABA-A agonist muscimol, to inactivate LIP specifically, and found only small biases (Zhou and Freedman, 2019) or no behavioral effects at all (Katz et al., 2016).

We hypothesized that the weak behavioral effects might be explained by compensation from unaffected parts of the decision-making network (Fetsch et al., 2018). Such compensation could arise from neurons in distal brain regions (including the homologous LIP in the opposite hemisphere) as well as from local neurons within the targeted LIP but outside the inactivated region. We therefore inactivated LIP, but in contrast to previous studies, we (1) ensured that our inactivation encompassed a substantial fraction of the neurons that were associated with decision formation, and (2) tracked the effect of inactivation over the course of each experimental session. Our results have shown



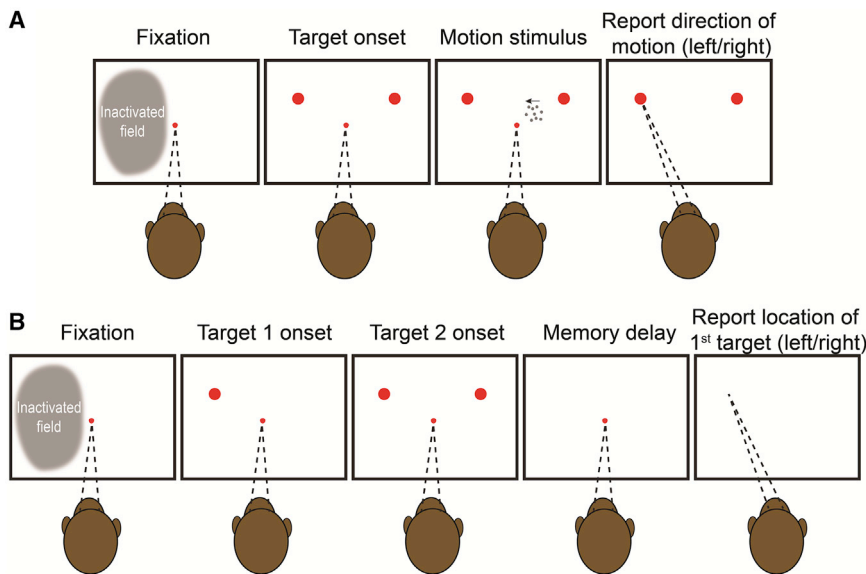


**Figure 1. Behavioral tasks**

(A and B) Both tasks require the monkey to make a binary decision and report it with an eye movement to one of two choice targets presented in the left or right hemifield. In each trial, the monkey is required to maintain its gaze on a central fixation point until its extinction, which serves as a *go cue*. (A) Motion direction task. Dynamic RDM appears within an invisible aperture contained within the hemifield ipsilateral to the inactivated cortex. The fixation point and motion stimulus are extinguished simultaneously, whereupon the monkey reports its decision. The monkey is rewarded for choosing the target in the direction of the motion (and randomly for the 0% coherent motion). Across trials, the strength, direction (left or right), and duration of the motion were varied randomly, as were the exact positions of choice targets (see Figure S1). (B) Temporal-order task. The choice targets are presented sequentially. Choice targets 1 and 2 are extinguished simultaneously, 430 ms after the onset of the first target. The fixation point is then extinguished after a variable delay, and the monkey is rewarded for making a saccade to the remembered location of the first target. Across trials, the order, onset asynchrony, and exact positions of the targets were varied randomly.

that inactivation of area LIP induced a significant bias in perceptual decisions but only temporarily; the bias diminished within a few hundred trials and across inactivation sessions. The behavioral compensation was evident in monkeys performing two types of decision-making tasks, highlighting the generality of the phenomenon.

## RESULTS

Here, we trained four rhesus monkeys on perceptual tasks requiring a binary decision about a stimulus category. Monkeys 1 and 2 had to decide whether the net direction of random dot motion (RDM) was to the left or right (Figure 1A). We varied the difficulty of the decision by controlling the strength and duration of the motion. After the removal of the motion stimulus, the monkeys reported the perceived net direction of motion with an eye movement to a choice target either on the right or left side of the display. Monkeys 3 and 4 had to decide on the temporal order of two flashed targets, which were presented sequentially in the left and right hemifield (Figure 1B). Difficulty was controlled by the time between the onset of the two targets ( $\Delta t$ ). After a wait period following target presentation, the monkeys had to report which of the two targets had appeared first by making an eye movement to the remembered location of that target.

The two tasks share the requirement of reporting the decision with an eye movement. In such tasks, neurons in area LIP that exhibit spatially selective persistent activity during saccade planning (Gnadt and Andersen, 1988) are believed to play a role in decision formation (Shadlen and Newsome, 1996; Wardak et al., 2002; Rorie et al., 2010). Here, we used a memory-guided saccade task (Gnadt and Andersen, 1988) to ascertain the full extent of LIP (in one hemisphere) that contains such neurons. Consistent with previous reports (Patel et al., 2010), neurons

with persistent activity were identified across a broad swath of the lateral bank of the intraparietal sulcus (IPS). The anteroposterior spread ranged from 6 to 10 mm; the dorsoventral spread ranged from 3 to 7 mm (Figures 2A and 2B). We targeted our inactivation to the region determined by this functional mapping in each monkey. In monkeys 1–3, we inactivated the region of interest by administering several injections of the GABA-A agonist muscimol. In monkey 4, we injected an adeno-associated virus (AAV) vector to express the inhibitory muscarinic receptor hM4Di in the region of interest (Armbruster et al., 2007) and activated the receptor by subcutaneous administration of clozapine. We confirmed that the inactivation encompassed the targeted area by multi-neuron recordings (Figures 2C and 2D).

In both tasks, the choice targets were in opposite hemifields, contralateral and ipsilateral to the inactivated area LIP. We refer to the corresponding choices as contraversive and ipsiversive, respectively. By convention, positive values of motion strength (task 1) and target asynchrony (task 2) indicate evidence for the contralateral choice target. Figure 3 shows the choice behavior over the first 100 trials of the first LIP inactivation experiment for each monkey. The rationale for restricting analysis to the earliest trials and sessions will be made clear in Figure 4. All monkeys made fewer contraversive choices during the 100 trials after inactivation than they did during the 100 trials before inactivation. This reduction held at nearly every stimulus strength in all four monkeys (Figure 3). Thus, the monkeys made more errors in response to contraversive motion (Figure 3A) and early contralateral target appearances (Figure 3B). This effect could not be attributed to more frequent fixation breaks on trials supporting a contralateral choice compared with an ipsilateral choice (Fisher exact test,  $p > 0.15$  for each monkey). The sigmoid curves in Figure 3 are fits of a logistic regression model (Equation 2). These fits show clear effects of

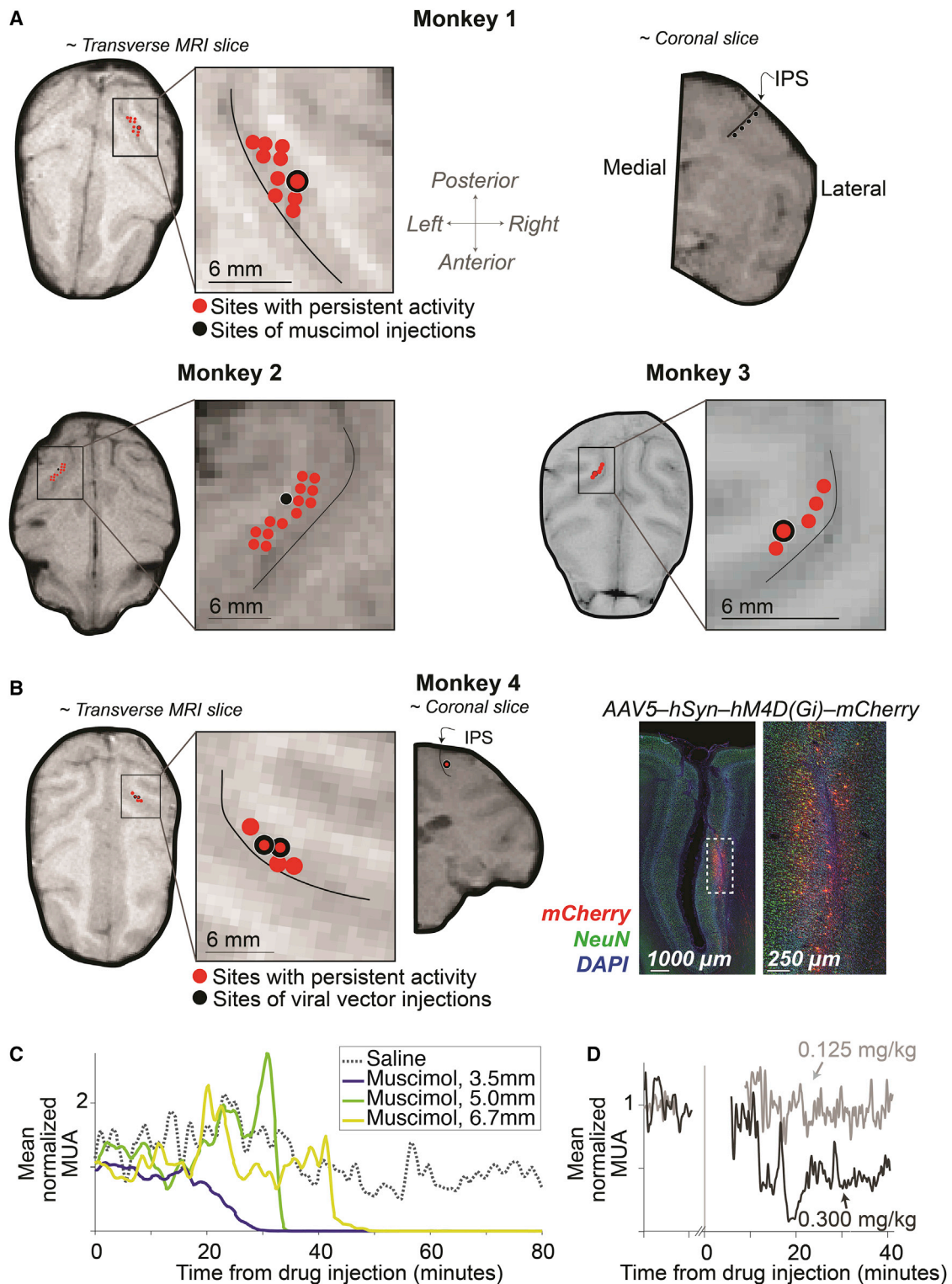


**Figure 2. Localization and characterization of LIP inactivation sites**

(A) The locations of muscimol injections and neurons with spatially selective persistent activity are superimposed on MRIs for monkeys 1, 2, and 3. The near-transverse planes are orthogonal to the injection trajectories. The near-coronal MRI slice from monkey 1 (top-right) shows positions along the intraparietal sulcus (IPS) where muscimol was injected. The thin black curve (inset) marks the center of the IPS.

(legend continued on next page)



muscimol and hM4Di-mediated inactivation on the monkeys' decisions compared with pre-inactivation and with control experiments. The dominant effect of inactivation is a bias against contraversive choices ( $p \leq 0.02$  in all cases; Table S1). Inactivation also appears to affect the slope of the choice functions, which would suggest decreased sensitivity to motion (monkey 1) and  $\Delta t$  (monkeys 3 and 4). The effect is statistically significant in monkey 3 ( $p < 0.01$ ; Table S2), and it is statistically significant in monkey 1 upon inclusion of more experimental sessions (Equation 9;  $p < 0.023$ ). Overall, however, the effect of inactivation on sensitivity was inconsistent across animals, and it is therefore difficult to interpret (Figure S3). From here on, we focus all analyses on the decision bias.

Inactivation with muscimol reduced contraversive choices in the first session, but this effect diminished over subsequent sessions. Figure 4A shows the bias during the first 100 trials in each muscimol session compared with controls. All three monkeys exhibited weaker biases against contraversive choices in later sessions. For monkey 1, the change is strictly monotonic, and for Monkey 3, nearly so ( $p = 10^{-4}$  and 0.003, respectively; Equation 6,  $\mathcal{H}_0 : \beta_2 = 0$ ). There is greater variability in monkey 2, but the decrease as a function of session number is statistically reliable ( $p = 0.01$ ). This effect is not explained by decreased efficacy of muscimol across sessions, as the drug induced silencing of neural activity in all sessions. Thus, the decision-making network can learn to compensate for the loss of area LIP across multiple days. For monkey 4, we varied the dosage of clozapine across sessions. As shown in Figure 4B, the contralateral bias was strongly dose dependent ( $p = 10^{-8}$ ). We did not detect an effect of session number in monkey 4 ( $p = 0.15$ ), possibly because it was masked by a strong effect of drug dosage, which was randomized across sessions. Also, we cannot ascertain whether the lack of across-session compensation is attributed to the chemogenetic approach, or to the limited number of sessions possible in this monkey, or to the confounding effect of clozapine dose.

In addition to the behavioral compensation observed across sessions, the bias also dissipated over the course of individual sessions. In most sessions, the bias decreased gradually over a few hundred trials and was nearly completely resolved by 500 trials (Figures 4C and 4D). Figures 4E and 4F highlight this within-session attenuation of bias by combining sessions in which a statistically significant bias was present in the first 100 trials (asterisks in Figures 4A and 4B). The initial bias is evident in the small fraction of correct contraversive choices ( $\sim 60\%$ ) and the large fraction of correct ipsiversive choices (80%–100%). This assay for the bias ignored stimulus strength, but it allowed us to focus on the effect of trial number within a session by pooling data over stimulus strengths and sessions. Thus, the running means reveal a gradual dissipation of the disparity be-

tween accuracy on the contralateral and ipsilateral supporting stimuli. These changes were highly reliable by logistic regression for three of the monkeys ( $p < 10^{-5}$ ; Equation 8,  $\mathcal{H}_0 : \beta_2 = 0$ ) and borderline for monkey 2 ( $p = 0.06$ ).

The behavioral compensation across trials was not caused by recovery of neural activity at the inactivated site, which persisted for the entire duration of each session (Figures 2C and 2D). Further, the monkeys still displayed signs of contralateral hemineglect on a simple extinction (side-preference) assay (Christopoulos et al., 2018a), conducted at the end of the experiment (monkeys 2 and 3). Both animals exhibited a strong bias for choosing the treat presented in the ipsilateral visual field (compared with control sessions,  $p < 10^{-3}$ , for both monkeys; Fisher exact test; Figure S2). Finally, inactivation of LIP did not induce significant contralateral deficits in saccade metrics in any of the monkeys (Figure S4). This indicates that the observed bias cannot be attributed to difficulty in making contralateral saccades, and the compensation of the bias could not be explained as a recovery of motor functions. Thus, the compensation exhibited on the perceptual decisions is task specific.

## DISCUSSION

Our study has shown that suppression of neural activity in cortical area LIP induces behavioral changes in perceptual decision-making. We used two types of behavioral tasks and two methods of inactivation. In all cases, inactivation of LIP in one hemisphere produced a bias against contraversive choices, consistent with partial spatial hemineglect (Mattingley et al., 1998). The effect was transient, however, bringing to light compensatory mechanisms that operate on at least two distinct timescales—over the course of a few hundred trials within individual sessions and across multiple sessions separated by days. Our results complement a previous study that reported an even faster, within-trial compensation, associated with optogenetic suppression of neurons in extrastriate cortical area MT (Fetsch et al., 2018).

Previous studies have shown that unilateral inactivation of LIP produces behavioral consequences consistent with contralateral hemineglect (Li et al., 1999; Chafee and Goldman-Rakic, 2000; Li and Andersen, 2001; Christopoulos et al., 2018b) and affects target selection in attentionally demanding tasks (Wardak et al., 2002, 2004). Our findings complement these studies by showing that LIP inactivation affects decisions in a manner similar to a change in base-rate, prior probability, or value differences (Hanks et al., 2011; Rorie et al., 2010; Platt and Glimcher, 1999). Also, the weak and inconsistent effects of inactivation on sensitivity are difficult to interpret. Unilateral inactivation leaves intact the other LIP, which is known to represent the evidence for and against both alternatives. Further note that if inactivation

(B) Left: location of viral vector injections for monkey 4. The red points in the MRI are sites containing neurons with spatially selective persistent activity. The coronal slice shows the injection site; same conventions as in (A). Right: representative histology. Expression of hM4Di-mCherry receptor is restricted to the lateral bank of the IPS.

(C) Time course of multi-unit activity (MUA) in area LIP following injection of saline (dotted) and muscimol (solid). Recordings were obtained at different distances from the injection site (legend). Note the complete suppression of activity in  $<1$  h. The post-drug testing session began 15 min after the completion of muscimol infusion (at least 1 h after the start of the infusion). See also Figure S2.

(D) Time course of MUA following subcutaneous injection of clozapine at the lowest (gray) and highest (black) dose tested.

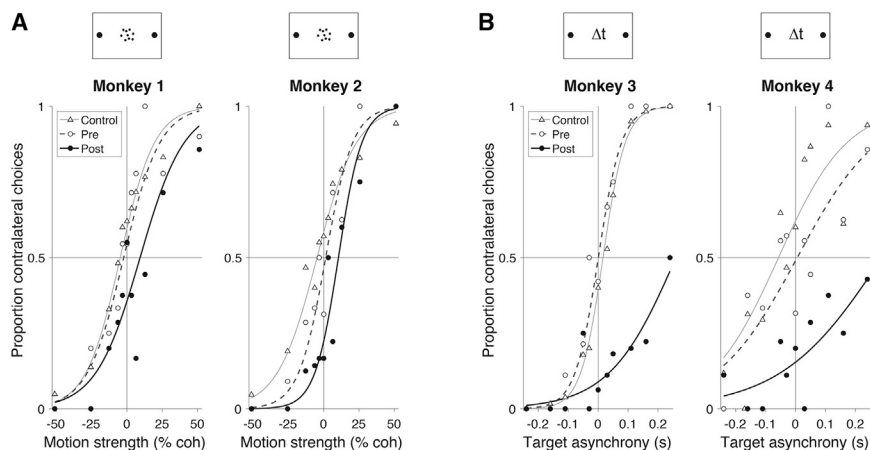


**Figure 3. Inactivation of LIP induces a decision bias**

(A) Proportion of contraversive choices as a function of motion strength for monkeys 1 and 2. Filled circles show data from the first 100 trials after muscimol injection in the first inactivation session. Open symbols show data from the last 100 trials in the pre-injection phase of the same experiments. Triangles depict data from all control sessions using the first 100 trials after the saline or sham injection. Muscimol induces a bias against contraversive choices. Curves are logistic regression fits (Equation 2).

(B) Proportion of contralateral choices as a function of target onset asynchrony for monkeys 3 and 4. Data from monkey 3 are from the first session in which muscimol was administered. Data from monkey 4 are from the session in which 0.3 mg/kg clozapine was administered. Other conventions are the same as in (A). See Tables S1 and S2 for statistical analysis.

were to produce weaker coherence-dependent signals in the spared tissue of the inactivated hemisphere, the main consequence would be a choice bias. For example, unilateral microstimulation of LIP biases decisions in favor of contraversive choices and does not affect sensitivity (Hanks et al., 2006). Indeed, the present findings would be unsurprising were it not for (1) the accompanying compensation and (2) two recent studies that reported such a bias to be absent (Katz et al., 2016) or vanishingly small (Zhou and Freedman, 2019). The present findings readily explain this discrepancy.

We attempted to inactivate the extent of area LIP that contains neurons with spatially selective persistent activity during the saccade planning phase of an oculomotor delayed response—neurons that have been shown to represent the accumulation of evidence during perceptual decision-making. Our mapping protocol revealed that the span of such neurons is extensive, consistent with Patel et al. (2010), indicating that a large injection of muscimol would be required to inactivate most of them. Thus, the volume of cortex inactivated in our experiments was  $\sim 1.5$  times the volume inactivated by Zhou and Freedman (2019) and Katz et al. (2016). We suspect that only a fraction of the relevant neurons were silenced in those studies, leaving open the possibility of weaker effects and more rapid compensation by neurons in the penumbra of the silenced tissue. Additional differences between these previous studies and ours may also contribute to the difference in results, including the levels of difficulty, jittering of the target positions, or differences in the motion display itself (e.g., highly salient moving elements in the Katz et al. study), which may discourage integration of evidence over time. Unless the animal is integrating information over time, relying on working memory (Constantinidis et al., 2018), or evaluating an interval of time itself (e.g., Leon and Shadlen, 2003), there is little reason to expect LIP to play a role in the decision.

It is notable that inactivation led to larger biases in the temporal-order task. The decision in both tasks manifests as a determination of which saccadic target is more likely to afford a liquid reward. The same statement can be rephrased in terms of relative salience or value of the choice targets. In the motion direc-

tion task, it is the motion patch in the unaffected, ipsilateral visual field that informs the relative affordances. In the temporal-order task, all relevant information derives from the targets themselves, one of which is in the affected hemifield. We suspect this difference underlies the more profound impairment in the temporal-order task. Indeed, at short  $\Delta t$ , the impairment mimics the double simultaneous stimulation test, used in bedside neurology to reveal extinction in the neglected hemifield. Importantly, despite these differences, compensation was present in both tasks.

The finding of compensation has broad implications for the interpretation of causal studies. Otchy et al. (2015) showed that successful inactivation experiments (i.e., leading to loss of function) need not implicate the brain tissue targeted by the causal intervention—related to the concept of *diaschisis* in neurology (Carrera and Tononi, 2014). Our finding adds the complementary caveat that inactivation experiments yielding negative results do not rule out a causal role of the inactivated tissue. In other words, causation does not imply necessity. Yet, the phenomenon of compensation is likely to play a more constructive role in neuroscience than muddying the interpretation of null inactivation experiments. Translational neuroscience stands to benefit greatly from a fuller characterization of behavioral compensation and its underlying mechanisms. This study and Fetsch et al. (2018) only begin to scratch the surface.

Notably, the present study does not address the mechanism underlying compensation. For example, we do not know if the compensation is mediated by portions of LIP outside the zone of inactivation, the contralateral LIP, or other association areas (e.g., frontal eye field and area 46) that contain neurons with response properties like area LIP (Kim and Shadlen, 1999; Funahashi et al., 1989; Ding and Gold, 2012). Rapid compensation would seem to rely on mechanisms of plasticity that operate on behaviorally relevant timescales (e.g., Magee and Grienberger, 2020). One possibility is that, shortly after LIP inactivation, downstream areas sense that the source of information they rely upon is compromised and establish communication with alternate sources. The mechanisms underlying such flexible

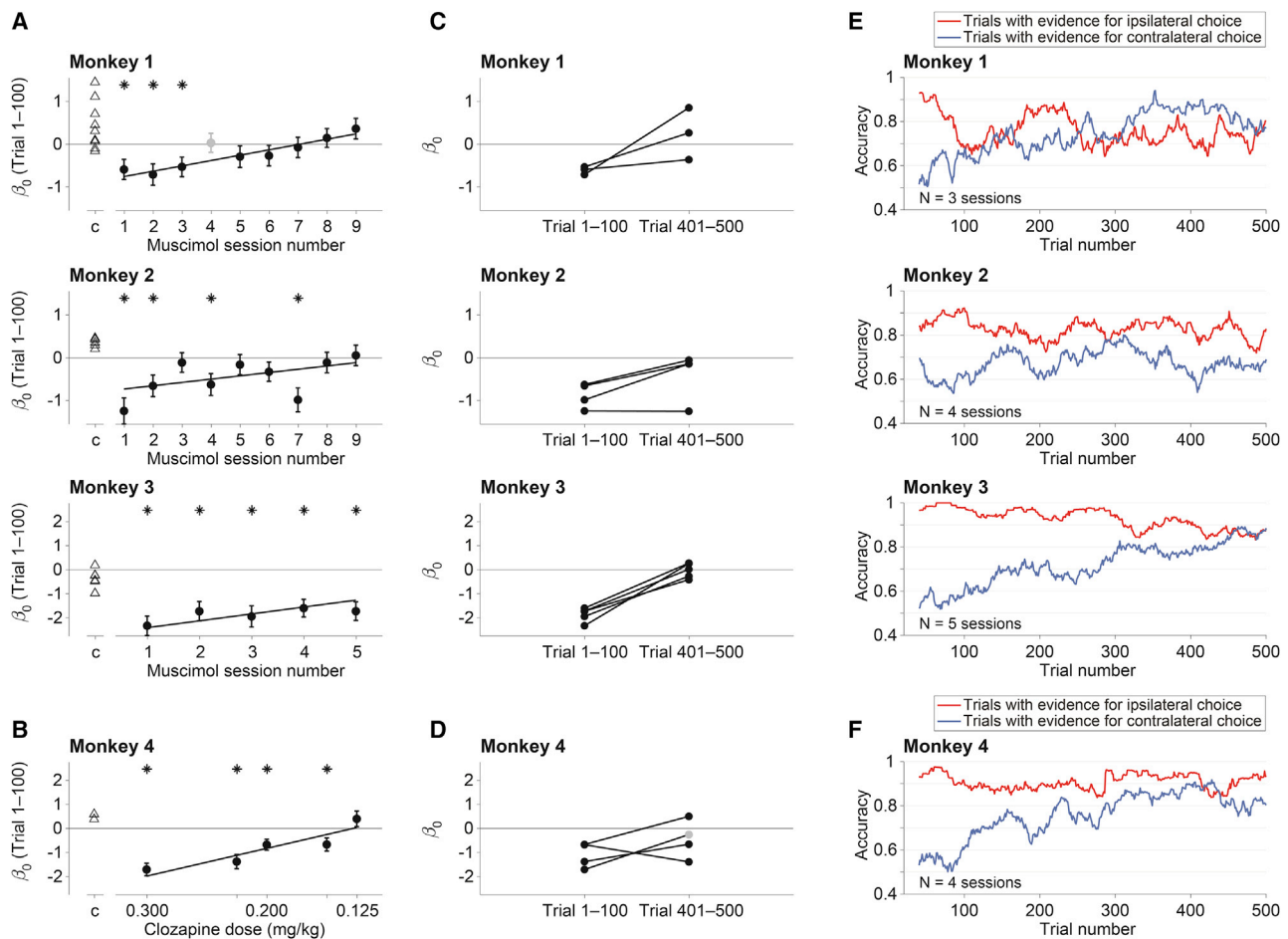


**Figure 4. Compensation of bias across and within sessions**

(A) The size of the contraversive bias ( $\beta_0$ ; Equation 2) in the first 100 trials following inactivation is plotted as a function of experimental session. Data are shown separately for the three monkeys that received muscimol. Negative bias ( $\beta_0 < 0$ ) indicates bias against contraversive decisions. Triangles are data from control sessions. Asterisks denote statistical significance ( $p < 0.05$ ;  $\mathcal{H}_0 : \beta_0 = 0$ ). The regression line is from the fit to Equation 6, excluding session 4 for monkey 1 (gray point), in which we injected a smaller volume (8  $\mu\text{L}$ ; see STAR Methods). Error bars are SE.

(B) Effect of clozapine dose on decision bias (monkey 4). Same conventions as in (A).

(C–F) Within-session compensation. These analyses use only sessions with a statistically significant bias in the first 100 trials (asterisks in A and B). See also Figure S3. (C) Individual muscimol sessions. Each line connects the bias in trials 1–100 with the bias in trials 401–500. (D) Individual clozapine sessions (monkey 4). Same conventions as in (C), except for one session, in which only 286 trials were completed. The gray point is the bias from the last 100 trials (trials 187–286). (E and F) Gradual diminution of the bias. These analyses combine the individual experiments in (C and D) and group trials with the same sign of evidence (color), regardless of evidence strength (trials with 0% coh or  $\Delta t = 0$  are excluded). The traces are running means of choice accuracy over 40 trials. Trial numbers on the abscissa correspond to the end of the averaging window.

routing of information from the senses to circuits that control behavior are unknown. Yet, they are essential for higher brain function for which dedicated input-output relations were not anticipated by evolution and therefore not determined by dedicated pathways. We suspect that these mechanisms involve both long-range cortico-cortical feedback and matrix thalamic projections to superficial cortical layers (e.g., Jones, 2001). The same mechanisms might underlie the resiliency of humans to focal cortical lesions (Cramer et al., 1997)—the clinical observation that small strokes are often silent until there are enough of them (e.g., vascular dementia). So the news is mixed. On the one hand, the possibility of compensation exposes the limitations of causal manipulation to assign cognitive functions to

localized regions of the brain. On the other hand, causal manipulations might be used to investigate the mechanism of compensation and to augment them to achieve clinically relevant goals.

### STAR★METHODS

Detailed methods are provided in the online version of this paper and include the following:

- KEY RESOURCES TABLE
- RESOURCE AVAILABILITY
  - Lead contact
  - Materials availability

- Data and code availability
- **EXPERIMENTAL MODEL AND SUBJECT DETAILS**
- **METHOD DETAILS**
  - Behavioral Tasks
  - Motion direction task
  - Temporal order task
  - Side-preference test
  - History of participation in experiments
  - Pharmacological inactivation and recordings
  - Chemogenetic inactivation and recordings
  - General procedures
- **QUANTIFICATION AND STATISTICAL ANALYSIS**
  - Behavioral data analysis
  - Eye movement analysis
  - Histology

### SUPPLEMENTAL INFORMATION

Supplemental information can be found online at <https://doi.org/10.1016/j.neuron.2022.03.022>.

### ACKNOWLEDGMENTS

We thank Anthony Napolitano, Brian Madeira, Cornel Duhaney, Lee Anthony Williams, and the Institute of Comparative Medicine for technical support and animal care; John Neumaier from the University of Washington for advice on chemogenetic techniques; and members of the Shadlen lab for helpful discussions.

The research was supported by the Howard Hughes Medical Institute; an R01 grant from the NIH Brain Initiative (M.N.S., R01NS113113); an R21 grant from the NIH National Institute on Aging (M.N.S., D.J., and S.S., 1R21AG067108); a postdoctoral fellowship from the Simons Collaboration on the Global Brain (Simons Foundation, D.J., 414196); a pilot grant from the Alzheimer's Disease Research Center at Columbia University (M.N.S., D.J., and S.S.); Young Investigator Awards from the Brain and Behavior Research Foundation (D.J., 28476 and S.S., 23556), and an R01 grant from the National Eye Institute (G.D.H., EY030441).

### AUTHOR CONTRIBUTIONS

Conceptualization, D.J., S.S., and M.N.S.; investigation, D.J., S.S., and Y.E.-S.; formal analysis, D.J., S.S., and M.N.S.; resources, G.D.H. and M.N.S.; writing – original draft, D.J., S.S., and M.N.S.; writing – review & editing, D.J., S.S., Y.E.-S., G.D.H., and M.N.S.; supervision, G.D.H. and M.N.S.; funding acquisition, D.J., S.S., G.D.H., and M.N.S.

### DECLARATION OF INTERESTS

The authors declare no competing interests.

### INCLUSION AND DIVERSITY

One or more of the authors of this paper self-identifies as an underrepresented ethnic minority in science. One or more of the authors of this paper received support from a program designed to increase minority representation in science.

Received: September 10, 2021  
Revised: January 3, 2022  
Accepted: March 12, 2022  
Published: April 13, 2022

### REFERENCES

Armbuster, B.N., Li, X., Pausch, M.H., Herlitze, S., and Roth, B.L. (2007). Evolving the lock to fit the key to create a family of G protein-coupled receptors

potently activated by an inert ligand. *Proc. Natl. Acad. Sci. USA* *104*, 5163–5168. <https://doi.org/10.1073/pnas.0700293104>. <http://www.ncbi.nlm.nih.gov/pubmed/17360345>.

Brainard, D.H. (1997). The psychophysics toolbox. *Spat. Vision* *10*, 433–436.

Carrera, E., and Tononi, G. (2014). Diaschisis: past, present, future. *Brain* *137*, 2408–2422.

Chafee, M.V., and Goldman-Rakic, P.S. (2000). Inactivation of parietal and prefrontal cortex reveals interdependence of neural activity during memory-guided saccades. *J. Neurophysiol.* *83*, 1550–1566. <http://www.ncbi.nlm.nih.gov/pubmed/10712479>.

Chen, X., Zirnsak, M., Vega, G.M., Govil, E., Lomber, S.G., and Moore, T. (2020). Parietal cortex regulates visual salience and salience-driven behavior. *Neuron* *106*, 177–187.e4. <https://doi.org/10.1016/j.neuron.2020.01.016>. <https://www.ncbi.nlm.nih.gov/pubmed/32048996>.

Christopoulos, V.N., Kagan, I., and Andersen, R.A. (2018). Lateral intraparietal area (LIP) is largely effector-specific in free-choice decisions. *Scientific Reports*, 1–13. <https://doi.org/10.1038/s41598-018-26366-9>.

Christopoulos, V.N., Andersen, K.N., and Andersen, R.A. (2018). Extinction as a deficit of the decision-making circuitry in the posterior parietal cortex. *Handbook of Clinical Neurology* *151*, 163–182.

Constantinidis, C., Funahashi, S., Lee, D., Murray, J.D., Qi, X.L., Wang, M., and Arnsten, A.F.T. (2018). Persistent spiking activity underlies working memory. *J. Neurosci.* *38*, 7020–7028.

Cramer, S.C., Nelles, G., Benson, R.R., Kaplan, J.D., Parker, R.A., Kwong, K.K., Kennedy, D.N., Finklestein, S.P., and Rosen, B.R. (1997). A functional MRI study of subjects recovered from hemiparetic stroke. *Stroke* *28*, 2518–2527. <https://doi.org/10.1161/01.str.28.12.2518>. <https://www.ncbi.nlm.nih.gov/pubmed/9412643>.

Ding, L., and Gold, J.I. (2010). Caudate encodes multiple computations for perceptual decisions. *J. Neurosci.* *30*, 15747–15759. <https://doi.org/10.1523/JNEUROSCI.2894-10.2010>. <https://www.ncbi.nlm.nih.gov/pubmed/21106814>.

Ding, L., and Gold, J.I. (2012). Neural correlates of perceptual decision making before, during, and after decision commitment in monkey frontal eye field. *Cereb. Cortex* *22*, 1052–1067. <https://doi.org/10.1093/cercor/bhr178>. <http://www.ncbi.nlm.nih.gov/pubmed/21765183>.

Fetsch, C.R., Kiani, R., Newsome, W.T., and Shadlen, M.N. (2014). Effects of cortical microstimulation on confidence in a perceptual decision. *Neuron* *83*, 797–804.

Fetsch, C.R., Odean, N.N., Jeurissen, D., El-Shamayleh, Y., Horwitz, G.D., and Shadlen, M.N. (2018). Focal optogenetic suppression in macaque area MT biases direction discrimination and decision confidence, but only transiently. *Elife* *7*, e36523. <https://doi.org/10.7554/eLife.36523>. <https://www.ncbi.nlm.nih.gov/pubmed/30051817>.

Funahashi, S., Bruce, C.J., and Goldman-Rakic, P.S. (1989). Mnemonic coding of visual space in the monkey's dorsolateral prefrontal cortex. *J. Neurophysiol.* *61*, 331–349.

Gnadt, J.W., and Andersen, R.A. (1988). Memory related motor planning activity in posterior parietal cortex of macaque. *Exp. Brain Res.* *70*, 216–220. <http://www.ncbi.nlm.nih.gov/pubmed/3402565>.

Gomez, J.L., Bonaventura, J., Lesniak, W., Mathews, W.B., Sysa-Shah, P., Rodriguez, L.A., Ellis, R.J., Richie, C.T., Harvey, B.K., Dannals, R.F., et al. (2017). Chemogenetics revealed: DREADD occupancy and activation via converted clozapine. *Science* *357*, 503–507. <https://doi.org/10.1126/science.aan2475>. <https://www.ncbi.nlm.nih.gov/pubmed/28774929>.

Hanks, T.D., Ditterich, J., and Shadlen, M.N. (2006). Microstimulation of macaque area LIP affects decision-making in a motion discrimination task. *Nat. Neurosci.* *9*, 682–689. <https://doi.org/10.1038/nn1683>.

Hanks, T.D., Mazurek, M.E., Kiani, R., Hopp, E., and Shadlen, M.N. (2011). Elapsed decision time affects the weighting of prior probability in a perceptual decision task. *J. Neurosci.* *31*, 6339–6352. <https://doi.org/10.1523/JNEUROSCI.5613-10.2011>. <http://www.ncbi.nlm.nih.gov/pubmed/21525274>.



- Hays, A.V., Richmond, B.J., and Optican, L.M. (1982). A UNIX-based multiple-process system for real-time data acquisition and control. *WESCON Conf. Proc. 2*, 1–10.
- Horwitz, G.D., Batista, A.P., and Newsome, W.T. (2004). Representation of an abstract perceptual decision in macaque superior colliculus. *J. Neurophysiol.* *91*, 2281–2296. <https://doi.org/10.1152/jn.00872.2003>. <http://www.ncbi.nlm.nih.gov/pubmed/14711971>.
- Jones, E.G. (2001). The thalamic matrix and thalamocortical synchrony. *Trends Neurosci* *24*, 595–601.
- Kass, R.E., and Raftery, A.E. (1995). Bayes factors. *J. Am. Stat. Assoc.* *90*, 773–795. <https://doi.org/10.1080/01621459.1995.10476572>.
- Katz, L.N., Yates, J.L., Pillow, J.W., and Huk, A.C. (2016). Dissociated functional significance of decision-related activity in the primate dorsal stream. *Nature* *535*, 285–288. <https://doi.org/10.1038/nature18617>. <https://www.ncbi.nlm.nih.gov/pubmed/27376476>.
- Kiani, R., Hanks, T.D., and Shadlen, M.N. (2008). Bounded integration in parietal cortex underlies decisions even when viewing duration is dictated by the environment. *J. Neurosci.* *28*, 3017–3029. <https://doi.org/10.1523/JNEUROSCI.4761-07.2008>. <http://www.ncbi.nlm.nih.gov/pubmed/18354005>.
- Kim, J.N., and Shadlen, M.N. (1999). Neural correlates of a decision in the dorsolateral prefrontal cortex of the macaque. *Nat. Neurosci.* *2*, 176–185. <https://doi.org/10.1038/5739>. <http://www.ncbi.nlm.nih.gov/pubmed/10195203>.
- Kleiner, M., Brainard, D., and Pelli, D. (2007). What's new in psychtoolbox-3? *Perception* *36*, 1–16.
- Leon, M.I., and Shadlen, M.N. (2003). Representation of time by neurons in the posterior parietal cortex of the macaque. *Neuron* *38*, 317–327.
- Li, C.S., and Andersen, R.A. (2001). Inactivation of macaque lateral intraparietal area delays initiation of the second saccade predominantly from contralateral eye positions in a double-saccade task. *Exp. Brain Res.* *137*, 45–57. <https://doi.org/10.1007/s002210000546>. <https://www.ncbi.nlm.nih.gov/pubmed/11310171>.
- Li, C.S., Mazzoni, P., and Andersen, R.A. (1999). Effect of reversible inactivation of macaque lateral intraparietal area on visual and memory saccades. *J. Neurophysiol.* *81*, 1827–1838. <https://doi.org/10.1152/jn.1999.81.4.1827>. <https://www.ncbi.nlm.nih.gov/pubmed/10200217>.
- Magee, J.C., and Grienberger, C. (2020). Synaptic plasticity forms and functions. *Annu. Rev. Neurosci.* *43*, 95–117. <https://doi.org/10.1146/annurev-neuro-090919-022842>.
- Mattingley, J.B., Husain, M., Rorden, C., Kennard, C., and Driver, J. (1998). Motor role of human inferior parietal lobe revealed in unilateral neglect patients. *Nature* *392*, 179–182. <https://doi.org/10.1038/32413>.
- National Research Council (2011). Guide for the care and use of laboratory animals, Eighth Edition (The National Academies Press). <https://doi.org/10.17226/12910>. <https://www.nap.edu/catalog/12910/guide-for-the-care-and-use-of-laboratory-animals-eighth>.
- Otchy, T.M., Wolff, S.B., Rhee, J.Y., Pehlevan, C., Kawai, R., Kempf, A., Gobes, S.M., and Ölveczky, B.P. (2015). Acute off-target effects of neural circuit manipulations. *Nature* *528*, 358–363. <https://doi.org/10.1038/nature16442>. <https://www.ncbi.nlm.nih.gov/pubmed/26649821>.
- Patel, G.H., Shulman, G.L., Baker, J.T., Akbudak, E., Snyder, A.Z., Snyder, L.H., and Corbetta, M. (2010). Topographic organization of macaque area LIP. *Proc. Natl. Acad. Sci. USA* *107*, 4728–4733. <https://doi.org/10.1073/pnas.0908092107>. <https://www.ncbi.nlm.nih.gov/pubmed/20173093>.
- Platt, M.L., and Glimcher, P.W. (1999). Neural correlates of decision variables in parietal cortex. *Nature* *400*, 233–238. <https://doi.org/10.1038/22268>. <http://www.ncbi.nlm.nih.gov/pubmed/10421364>.
- Raper, J., Morrison, R.D., Daniels, J.S., Howell, L., Bachevalier, J., Wichmann, T., and Galvan, A. (2017). Metabolism and distribution of clozapine-n-oxide: implications for nonhuman primate chemogenetics. *ACS Chem. Neurosci.* *8*, 1570–1576. <https://doi.org/10.1021/acscchemneuro.7b00079>. <https://www.ncbi.nlm.nih.gov/pubmed/28324647>.
- Roitman, J.D., and Shadlen, M.N. (2002). Response of neurons in the lateral intraparietal area during a combined visual discrimination reaction time task. *J. Neurosci.* *22*, 9475–9489. <http://www.ncbi.nlm.nih.gov/pubmed/12417672>.
- Rorie, A.E., Gao, J., McClelland, J.L., and Newsome, W.T. (2010). Integration of sensory and reward information during perceptual decision-making in lateral intraparietal cortex (LIP) of the macaque monkey. *PLoS One* *5*, e9308. <https://doi.org/10.1371/journal.pone.0009308>. <https://www.ncbi.nlm.nih.gov/pubmed/20174574>.
- Shadlen, M.N., and Kiani, R. (2013). Decision making as a window on cognition. *Neuron* *80*, 791–806. <https://doi.org/10.1016/j.neuron.2013.10.047>. <http://www.ncbi.nlm.nih.gov/pubmed/24183028>.
- Shadlen, M.N., and Newsome, W.T. (1996). Motion perception: seeing and deciding. *Proc. Natl. Acad. Sci. USA* *93*, 628–633. <http://www.ncbi.nlm.nih.gov/pubmed/8570606>.
- Wardak, C., Olivier, E., and Duhamel, J.R. (2002). Saccadic target selection deficits after lateral intraparietal area inactivation in monkeys. *J. Neurosci.* *22*, 9877–9884. <https://www.ncbi.nlm.nih.gov/pubmed/12427844>.
- Wardak, C., Olivier, E., and Duhamel, J.R. (2004). A deficit in covert attention after parietal cortex inactivation in the monkey. *Neuron* *42*, 501–508. [https://doi.org/10.1016/S0896-6273\(04\)00185-0](https://doi.org/10.1016/S0896-6273(04)00185-0). <https://www.ncbi.nlm.nih.gov/pubmed/15134645>.
- Zhou, Y., and Freedman, D.J. (2019). Posterior parietal cortex plays a causal role in perceptual and categorical decisions. *Science* *365*, 180–185. <https://doi.org/10.1126/science.aaw8347>. <https://www.ncbi.nlm.nih.gov/pubmed/31296771>.

## STAR★METHODS

### KEY RESOURCES TABLE

REAGENT or RESOURCE	SOURCE	IDENTIFIER
<b>Antibodies</b>		
Anti-mCherry (rabbit, polyclonal)	GeneTex	GTX59788 RRID: AB_10721869
Anti-NeuN (mouse, monoclonal)	Millipore	MAB377 RRID: AB_2298772
Donkey anti-Rabbit IgG (H+L) Highly Cross-Adsorbed Secondary Antibody, Alexa Fluor 568	Invitrogen Molecular Probes	A10042 RRID: AB_2534017
Donkey anti-Rabbit IgG (H+L) Highly Cross-Adsorbed Secondary Antibody, Alexa Fluor 488	Invitrogen Molecular Probes	A21206 RRID: AB_141708
<b>Bacterial and virus strains</b>		
AAV5-hSyn-hM4Di-mCherry	Addgene	RRID: Addgene_50475
<b>Chemicals, peptides, and recombinant proteins</b>		
Clozapine	Hello Bio	HB1607
<b>Deposited data</b>		
Behavioral data	This paper	<a href="https://doi.org/10.17632/86nb57ckv9.1">https://doi.org/10.17632/86nb57ckv9.1</a>
<b>Experimental models: Organisms/strains</b>		
Macaca mulatta	Washington National Primate Research Center	N/A
<b>Software and algorithms</b>		
Matlab	Mathworks Inc.	N/A
Analysis code	This paper	URL: <a href="https://github.com/DaniqueJeurissen/Jeurissen_Shushruth_etal_2022_Neuron">https://github.com/DaniqueJeurissen/Jeurissen_Shushruth_etal_2022_Neuron</a> <a href="https://doi.org/10.5281/zenodo.6348004">https://doi.org/10.5281/zenodo.6348004</a>

### RESOURCE AVAILABILITY

#### Lead contact

Further information and requests for resources and reagents should be directed to and will be fulfilled by the lead contact, Michael N. Shadlen ([shadlen@columbia.edu](mailto:shadlen@columbia.edu)).

#### Materials availability

This study did not generate new unique reagents.

#### Data and code availability

- Behavioral data have been deposited to Mendeley Data and are publicly available as of the date of publication. DOI is listed in the [key resources table](#).
- Code to analyze the data has been deposited in a Github repository and is publicly available as of the date of publication. URL is listed in the [key resources table](#).
- Any additional information required to reanalyze the data reported in this paper is available from the [lead contact](#) upon request.

### EXPERIMENTAL MODEL AND SUBJECT DETAILS

All training, surgery, and experimental procedures were conducted in accordance with the Public Health Service Policy on Humane Care and Use of Laboratory Animals ([National Research Council, 2011](#)). Experiments were approved by the Columbia University Institutional Animal Care and Use Committee (IACUC) under protocol number AC-AAAW4454.

We performed extracellular neural recordings and unilateral reversible inactivation in the parietal cortex of four adult male rhesus macaques. The animals weighed 10, 7, 10, and 8 kg, and were aged 9, 18, 18, and 12 years, respectively. We used a pharmacological approach for inactivation in monkeys 1, 2, and 3 and a chemogenetic approach in monkey 4. All four monkeys had a headpost to

allow head fixation and a CILUX recording chamber (Crist Instruments) over the parietal cortex. Recording chambers provided access to the right hemisphere in monkeys 1 and 4 and to the left hemisphere in monkeys 2 and 3.

## METHOD DETAILS

### Behavioral Tasks

Visual stimuli were presented on a CRT monitor (60 or 75 Hz refresh rate; viewing distance 58 or 48 cm). Eye position was recorded using an infrared eye tracker (Eyelink, SR Research; sampling rate: 1 kHz). Stimuli were generated using the Psychophysics Toolbox (Brainard, 1997; Kleiner et al., 2007) in Matlab (Mathworks) under the control of a PC running the real time experimental control system (ReX; Hays et al., 1982) under the QNX operating system. Juice rewards were delivered by a solenoid-based reward system.

Many task events are separated by random durations drawn from a truncated exponential distribution

$$f(t) = \begin{cases} \frac{\alpha}{\lambda} e^{-\frac{t-t_{\min}}{\lambda}} & t_{\min} \leq t \leq t_{\max} \\ 0 & \text{otherwise} \end{cases} \quad (\text{Equation 1})$$

where  $t_{\min}$  and  $t_{\max}$  define the range,  $\lambda$  is the time constant, and  $\alpha$  is chosen to ensure the total probability is unity. Below, we report the range and the exponential parameter  $\lambda$ . Because of truncation, the expectation  $\mathbb{E}(t) < \lambda$ .

### Motion direction task

Monkeys 1 and 2 were required to decide whether the net direction of motion in a dynamic random dot display was leftward or rightward (Figure 1A). The animal initiated each trial by fixating within  $\pm 4$  degrees visual angle (dva) of a central red fixation point on a black background. After 0.6–1 s, two red choice-targets appeared in the left and right upper quadrants of the visual field. The exact location of each target was chosen randomly and independently on each trial using a uniform distribution of polar angle and eccentricities within a specified range (see Figure S1). We took this step to ensure that the monkey could not infer the location of one target from the location of the other. After a delay (range: 0.8–1.5 s,  $\lambda=1$ ; Equation 1), the RDM stimulus appeared within a circular aperture (radius: 2.5 dva), centered 3.5 dva from the fixation point. The RDM was confined to the hemifield ipsilateral to the inactivated LIP, and this location was constant across training, drug, and control sessions. The RDM was generated using previously described methods (Roitman and Shadlen, 2002). Three interleaved sets of dots (density 16.7 dots/deg<sup>2</sup>/s) were presented on successive video frames. Each dot was redrawn three video frames later at a random location within the stimulus aperture or at a location consistent with the direction of motion; the motion coherence is the probability of the latter occurring. The coherence on each trial was drawn randomly from the set  $\pm[0, 0.032, 0.064, 0.128, 0.256, 0.512]$ . Positive values indicate that the motion was towards the target in the hemifield contralateral to the inactivation site; negative values indicate motion towards the target in the ipsilateral hemifield. On 0% motion coherence trials, one of the targets was randomly assigned as correct. The RDM was presented for a variable duration (range: 0.1–2 s,  $\lambda=0.3$ ; Equation 1). The fixation point and RDM disappeared simultaneously, whereupon the monkey was allowed to indicate its decision about the direction of motion by making a saccade to the corresponding target.

For monkey 1, we used a fixed ratio reward schedule with a juice reward for every correct trial. For monkey 2 we used a variable ratio reward schedule with a juice reward for only a subset of the correct trials. The number of correct trials needed to obtain a reward was a random number drawn from a Normal distribution,  $\mathcal{N}\{3, 1\}$ , and discretized to the nearest integer from 1–6. Incorrect trials were never rewarded and were followed by a time-out (5 s).

### Temporal order task

Monkeys 3 and 4 performed a temporal-order discrimination task in which they indicated which of two targets appeared first (Figure 1B). The animal initiated a trial by acquiring a central red fixation point. After 0.6–1 s of maintained fixation, two targets appeared, one in each hemifield at locations that were randomized across trials, as in the motion task (Figure S1). The delay between targets was randomly chosen on each trial from the set  $\pm [0, 27, 53, 107, 160, 240]$  ms, where positive values indicate that the target contralateral to the inactivated side was presented first. The first target stayed on the screen for 0.43 s, and both targets disappeared simultaneously. Following a memory delay (drawn from a truncated exponential distribution, range 1–2 s,  $\lambda=1.4$ ), the monkey was required to make a saccade to the remembered location of the target that had appeared first to obtain a juice reward. Both monkeys were rewarded using a fixed ratio reward schedule with a juice reward for all correct trials and on 50% of the trials in which the targets appeared simultaneously.

### Side-preference test

Monkeys 2 and 3 were tested for signs of spatial hemineglect (Christopoulos et al., 2018a) at the end of experimental sessions. The testing was performed after retraction of any pipettes and electrodes in the brain but before the head fixation was released. Two equal sized pieces of fruit were offered to the monkey, one to the left and another to the right, equidistant from the mouth. The animal indicated its choice for one piece of fruit by extending its tongue to one side or the other to acquire that treat. This procedure was repeated 8–16 times per session. A Fisher exact test was used to compare the proportion of ipsilateral choices between tests conducted after inactivation sessions and after control sessions (Figure S2). On interleaved control trials, a single piece of fruit was offered unilaterally to confirm that the monkey could indicate choices on both sides.

### History of participation in experiments

Three of the monkeys had participated in other causal manipulation experiments. We provide details here for completeness. Monkeys 1 and 2 had participated in an experiment in which small clusters of cells in area MT were inhibited using optogenetics (Fetsch et al., 2018) or stimulated using electrical stimulation (Fetsch et al., 2014) in a post-decision wagering task. Before training on the temporal-order discrimination task and before the injection of the viral vectors, Monkey 4 participated in 5 sessions in which we optimized our muscimol infusion techniques. During these sessions, muscimol was infused into area LIP while the monkey performed simple saccadic tasks.

### Pharmacological inactivation and recordings

We used magnetic resonance imaging (MRI) to localize the intraparietal sulcus (IPS) in relation to the recording chamber. We obtained MR images (T1 weighted gradient-echo sequences in monkeys 1, 2, and 4; a T2 weighted spin-echo sequence in monkey 3) with a recording grid *in situ*. We used custom software to project the recording grid onto the MR images (Figures 2A and 2B). We systematically mapped the lateral bank of the IPS (sampling every 300–500  $\mu\text{m}$ ) and noted the locations of neurons with spatially selective persistent activity during visually guided and memory-guided saccade tasks (Gnadt and Andersen, 1988). We planned our inactivation to encompass as many of these locations as possible.

Muscimol and saline injections were made with quartz glass injection pipettes (115  $\mu\text{m}$  outer diameter, 85  $\mu\text{m}$  inner diameter, beveled tip, Thomas Recording). Extracellular neural recordings were obtained with a tungsten microelectrode (100  $\mu\text{m}$  outer diameter,  $\approx 1\text{ M}\Omega$  impedance, FHC Inc.) to confirm tissue silencing (Figure 2C) and to estimate its spatial extent. The pipette and the microelectrode were advanced independently using a motorized hydraulic drive (Narishige International Inc.) along parallel trajectories through the IPS. The mean distance between the electrode and first injection site was 3.6 mm (range of 2.1–6.7 mm across sessions). A grid system allowed us to place the pipette at a site with an abundance of the targeted neurons and sufficiently near other targeted sites to achieve inactivation by diffusion from multiple injections spaced along this single trajectory (see Figure 2A; Table S3). The injection site and depths were the same in all sessions for a given monkey.

The location of the recording electrode varied across sessions but was always at a location on the lateral bank of the IPS with strong multi-unit neural activity (MUA) before inactivation. We quantified the MUA (Figures 2C and 2D) as follows. The raw voltage signal (30 kHz sampling rate) was bandpassed between 300 Hz and 6 kHz. The mean and standard deviation ( $\sigma$ ) of the filtered signal in the time window 90 s before initiation of inactivation established a baseline for comparison. The raw MUA is defined as the frequency of positive crossings of threshold  $3\sigma$  above baseline. Figures 2C and 2D show the MUA normalized to the average MUA during the baseline epoch. The electrode was left in place while the monkeys performed the task to confirm that the tissue remained inactivated.

Injections were made with a Hamilton syringe (1700 series, gas tight, 50  $\mu\text{L}$  volume) using a micro-injection pump (Phd Ultra-nanomite, Harvard Apparatus Inc.) connected to the pipette with Tygon tubing (0.25 mm inner diameter). The Hamilton syringe was filled with silicone fluid (Octamethyltrisiloxane; Clearco Products) mixed with fluorescent leak-detection dye (Dye-Lite; Tracerline) and filter-sterilized by passage through a Mixed Cellulose Esters membrane (Millex-GS 0.22  $\mu\text{m}$ ; SLGS033SB; EMD Millipore). The dyed silicone fluid allowed visualization of the meniscus to confirm the injected volume based on the length of travel of dye along the tubing.

We infused muscimol (8  $\mu\text{g}/\mu\text{L} \times 0.4\ \mu\text{L}/\text{min}$ ) at four depths along the injection track. The first of the four injections made during each session was at the deepest target location. After each injection, the pipette was left in place for at least 5 minutes before retraction to the next injection site. After each session, we confirmed that the pipette was intact by turning the pump on and visualizing a drop of fluid at the pipette tip. Table S3 shows injection details for the individual sessions. The total volume was typically 20  $\mu\text{L}$  per session. However, in the first session (Monkey 1) the total volume was 45  $\mu\text{L}$ , and in the fourth session the total volume was 8  $\mu\text{L}$ . The low-volume injection failed to induce behavioral effects and we reverted to 20  $\mu\text{L}$  in subsequent sessions. This session is excluded from the analysis in Figure 4A, but the reported effect is statistically significant with this data point included. We had to terminate data collection from Monkey 3 early due to the SARS-CoV-2 pandemic (summer 2020).

Saline injections followed the same injection protocol. We limited the number of saline injections to avoid tissue damage at the injection site (Zhou and Freedman, 2019). In sham sessions, all procedures were identical to those used in the muscimol and saline injections except that the pipette remained in the guide tube instead of being lowered into the brain, and the syringe was not connected to the pipette. In some sham sessions, we did not lower the electrode into the brain. We refer to both saline injections and sham sessions as control sessions.

### Chemogenetic inactivation and recordings

In monkey 4, we injected the viral vector AAV5-hSyn-hM4Di-mCherry (titer =  $4.9 \times 10^{12}$  genome copies/mL, RRID: Addgene\_50475) at locations informed by the mapping experiments (Figure 2B). Injection procedures were similar to those described above for drug injections. The differences are detailed here. The viral vector was administered with a custom injectrode, comprising a pipette affixed to an electrode that protruded 700–800  $\mu\text{m}$  beyond the tip of the pipette. The injectrode was lowered into the brain through a single transdural guide tube using a motorized hydraulic drive (FHC Inc.). Before injecting, we confirmed that the injectrode was at a location where neurons showed persistent activity during saccadic tasks. Injections were made along two tracks, separated by 1.4 mm, on two consecutive days. Each day, we injected at 13–14 depths separated by 500  $\mu\text{m}$  covering 5.5–6 mm. We injected 0.5  $\mu\text{L}$  at each location at a rate of 0.1  $\mu\text{L}/\text{min}$ , starting at the deepest location. The total injected volume was 13.5  $\mu\text{L}$ . After each injection, the injectrode was left in place for an additional 8 minutes before being retracted to the next site. We then waited 6 months for expression of the hM4Di receptor to stabilize before beginning behavioral experiments.



In the inactivation experiments, we administered the hM4Di agonist, clozapine (Hello Bio #HB1607, concentrations listed in Table S3). Clozapine was chosen over the designer drug CNO as it is a more potent agonist of hM4Di receptors in the central nervous system at doses less than 10% of the minimum dose used clinically (Gomez et al., 2017; Raper et al., 2017). The monkey was trained to present its right arm through an opening in the primate chair to allow for subcutaneous clozapine injection. During two inactivation sessions, we recorded the effect of clozapine administration on neural firing rate with 24-channel V-probes (Plexon Inc.). The V-probe recordings were made 1–1.4 mm from the the viral injections. Following the session in which clozapine was administered at 0.15 mg/kg (see Table S3), monkey 4 lost the cranial implant that allowed head stabilization. Subsequently, we were able to collect data from two additional inactivation sessions and two control sessions using a noninvasive restraint system.

### General procedures

During experimental sessions, the recording electrode was lowered into the brain and left in place until the end of the session. Baseline behavioral data were collected for at least 200 trials of the relevant task (motion direction or temporal order task). For Monkey 1 and 4, we then initiated the relevant inactivation procedure. For monkey 2 and 3, we used inclusion criteria based on psychometric data to decide whether the behavior was sufficiently stable to continue the experiment. We computed the subjective point of equality (SPE) from logistic fit to the choice data ( $-\beta_1/\beta_0$  from Equation 2). Monkey 2 would continue the session only if  $|\text{SPE}| \leq 3.2\%$  coherence and the error rate at the highest coherence was  $\leq 5\%$ . For Monkey 3 the criteria were  $|\text{SPE}| \leq 0.026$  seconds and error rate  $\leq 5\%$ . Based on these inclusion criteria, we aborted 7 sessions for Monkey 2, and 7 sessions for Monkey 3.

During muscimol administration, the animals watched cartoon movies and received occasional juice rewards for looking at the screen. The pipette was left in place for at least 15 minutes afterwards, and behavioral data collection resumed after pipette removal. In the chemogenetic inactivation sessions, the animal waited for at least 30 minutes after clozapine administration before the collection of behavioral data resumed. In most sessions, monkeys performed at least 500 trials following inactivation. These 500 trials were included in the post-inactivation analysis. At the conclusion of each session and after removing the electrode and pipette from the chamber, we collected data in the extinction task (monkeys 2 and 3 only). After each inactivation session, the animal did not work on any task for at least 3 days.

## QUANTIFICATION AND STATISTICAL ANALYSIS

### Behavioral data analysis

We analyzed the effect of inactivation on choice using a variety of generalized linear models (GLM; logistic regression). The simplest generates the fits in Figure 3.

$$\text{logit}[p^+(s)] = \theta = \beta_0 + \beta_1 s \quad (\text{Equation 2})$$

$$p^+(s) = \frac{e^\theta}{1 + e^\theta} \quad (\text{Equation 3})$$

where  $p^+$  is the probability of a contraversive choice and  $s$  is the signed motion coherence (motion direction task) or the signed  $\Delta t$  (temporal order task). In all cases,  $s > 0$  indicates support for the choice target in the hemifield contralateral to the site of inactivation.

In the motion task, the strength of motion is a function of the coherence (coh) of the RDM stimulus and the duration of the presentation,  $t$ . The strength of the stimulus is therefore captured by a power law

$$s_t = \text{coh} \times t^\pi \quad (\text{Equation 4})$$

For perfect, unbounded accumulation of independent samples, the exponent would be  $\pi = 0.5$ , (i.e., the rate of improvement of signal to noise in the accumulation of independent identically distributed random samples), but the presence of a terminating bound attenuates the improvement (Kiani et al., 2008). The exponent used here was derived by fitting Equation 2, with  $s = s_t$ , to the control data ( $\pi = 0.38$  and  $0.43$  for monkeys 1 and 2, respectively). Using pre-injection data from all sessions, we confirmed that the version of Equation 2 with  $s_t$  is superior to a model that ignores stimulus duration ( $\Delta\text{BIC} = 31$  for monkey 1 and  $27$  for monkey 2; *strong* support; Kass and Raftery, 1995). We use Equation 4 for all statistical analyses of the motion experiments. For the asynchrony experiment  $s_t = \Delta t = s$ , as defined above. Significance tests are standard t-tests, based on the standard error of the parameter, or  $\chi^2$ -tests, based on the difference in the deviance of nested models with and without the terms that define the null hypothesis,  $\mathcal{H}_0$ .

For comparing inactivation-induced bias to pre-existing bias (in the same session) or to the bias on comparable trials during control sessions, we used the GLM,

$$\text{logit}[p^+(s_t, I_\emptyset)] = \beta_0 + \beta_1 s_t + \beta_2 I_\emptyset + \beta_3 s_t I_\emptyset \quad (\text{Equation 5})$$

where  $I_\emptyset = 1$  if the trial occurs after administration of muscimol or clozapine, and 0 otherwise. To test whether inactivation produces a bias against contralateral choices, the null hypothesis is  $\{\mathcal{H}_0 : \beta_2 = 0\}$ . The curves shown in Figure 3A use the expectation of  $s_t$ :

$$\mathbb{E}[s_t] = \text{coh} \times \int_{t_{\min}}^{t_{\max}} f(t) t^\pi dt$$

where  $f(t)$  is the distribution of durations defined in Equation 1 and  $\pi$  takes the values defined above.

### Change in bias across sessions

To visualize compensation across sessions in monkeys 1–3 (Figure 4A) and across clozapine dosage in monkey 4 (Figure 4B) we used the GLM:

$$\text{logit}[p^+(s_t, S_x)] = \beta_0 + \beta_1 s_t + \beta_2 S_x \quad (\text{Equation 6})$$

where  $S_x$  is either the  $x^{\text{th}}$  session number in chronological order (for monkeys 1–3) or the dose of administered clozapine in mg/kg (for monkey 4). For this analysis we use only the first 100 trials after inactivation. Lines in Figures 4A and 4B are from this fit as are the  $p$ -values reported in results. We confirmed that the effect of session number (or clozapine dose) on behavior is statistically significant even when the following saturated model was considered:

$$\text{logit}[p^+(s_t, S_x)] = \beta_0 + \beta_1 s_t + \beta_2 S_x + \beta_3 s_t S_x \quad (\text{Equation 7})$$

### Change in bias during a session

To visualize the decay of the choice bias over the course of a session (Figures 4C and 4D), we compared  $\beta_0$  terms for Equation 2, computed from trials 1–100 and from trials 401–500 (or the last 100 trials if the animal did not complete a 500 trial block after inactivation). Due to compensation across sessions, we could not detect a bias post-inactivation in some of the later sessions. We therefore only analyze sessions in which there was a significant bias in the first 100 trials. To compute the rate of compensation across trials in individual sessions, we added the term  $N_{\emptyset}$ , the trial number after inactivation, to Equation 2:

$$\text{logit}[p^+(s_t, N_{\emptyset})] = \beta_0 + \beta_1 s_t + \beta_2 N_{\emptyset} \quad (\text{Equation 8})$$

Finally, the statement about the effect of inactivation on sensitivity (monkey 1) is supported by combining the first three inactivation sessions and elaborating Equation 5 to include the trial number (post-injection) in each session:

$$\text{logit}[p^+(s_t, I_{\emptyset})] = \beta_0 + \beta_1 s_t + \beta_2 I_{\emptyset} + \beta_3 s_t I_{\emptyset} + \beta_4 N_{\emptyset} + \beta_5 s_t N_{\emptyset} \quad (\text{Equation 9})$$

We report the  $p$ -value associated with  $\{H_0 : \beta_3 = \beta_5 = 0\}$ , using the last 100 pre-injection trials and the first 500 post-injection trials from each session.

### Eye movement analysis

Eye position was continually recorded at a sampling rate of 1 kHz. For monkeys 1 to 3, we analyzed the first 100 trials post inactivation from the first two muscimol infusion sessions and from the two control sessions conducted closest to the inactivation sessions. For monkey 4, we used data from the sessions in which a high dose of clozapine (0.225 and 0.2 mg/kg) had been administered and from adjacent control sessions. For the analysis summarized in Figure S4 we considered three saccadic metrics: the latency from offset of the fixation point to saccade initiation, peak velocity, and the distance between the endpoint and the choice target (end point error). The distribution of saccade metrics for the control and drug condition trials were compared separately for ipsilateral and contralateral choices with a Rank Sum test. An ANOVA was used to determine the statistical significance of the interaction between choices and drug conditions.

$$Y = \beta_0 + \beta_1 I_s + \beta_2 I_d + \beta_3 I_s I_d \quad (\text{Equation 10})$$

where  $Y$  is the saccadic metric and the  $I_x$  terms are indicator variables for side of saccade direction and inactivation:

$$I_s = \begin{cases} 1 & \text{contra saccade} \\ 0 & \text{ipsi saccade} \end{cases} \quad I_d = \begin{cases} 1 & \text{inactivation} \\ 0 & \text{control} \end{cases}$$

We report  $p$ -values associated with null hypothesis,  $H_0 : \beta_3 = 0$ .

### Histology

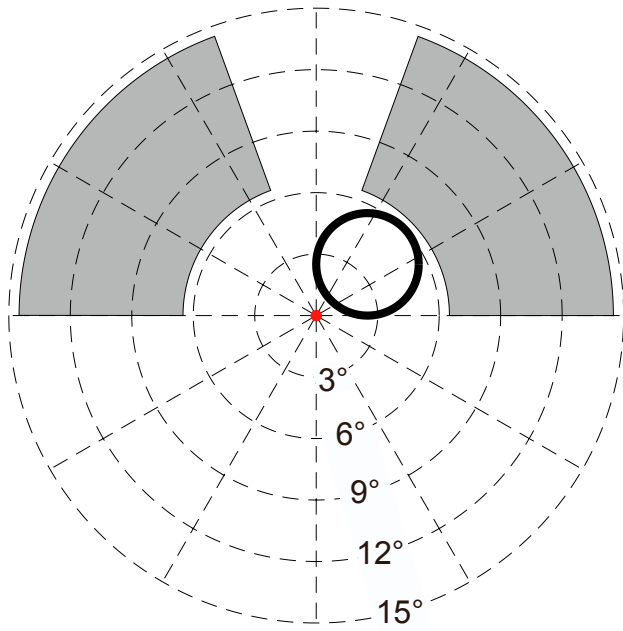
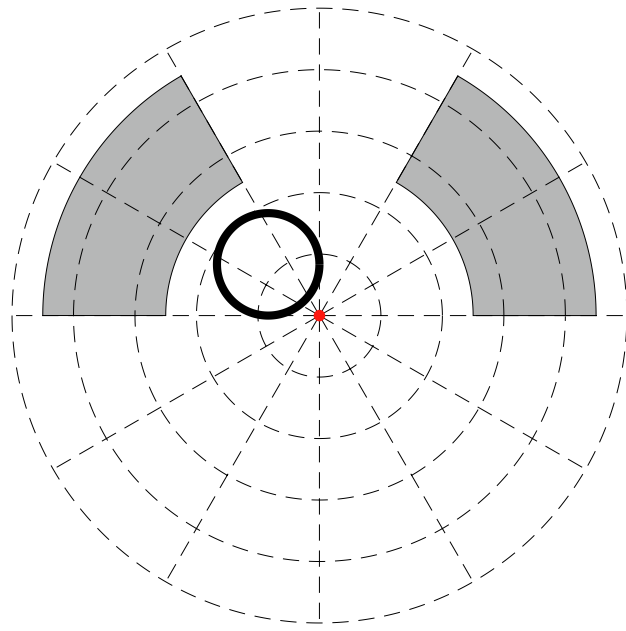
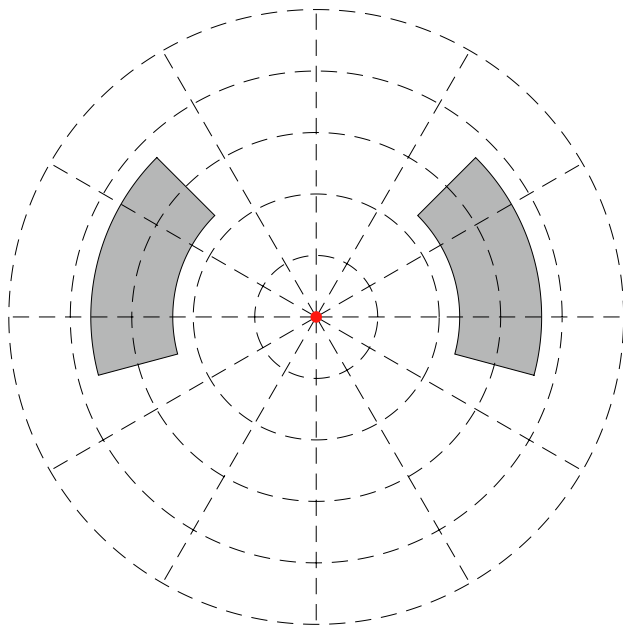
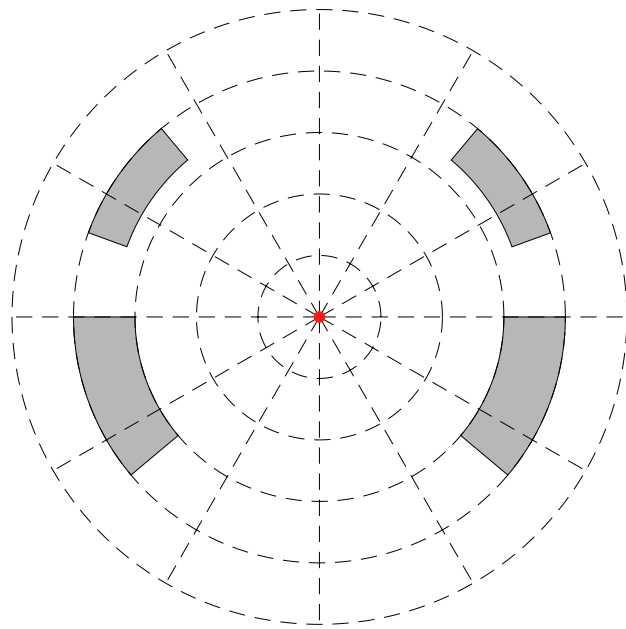
We verified expression of the hM4Di-receptor in monkey 4 histologically. The animal was euthanized under deep isoflurane anesthesia and perfused transcardially with 4% paraformaldehyde followed by a gradient of sucrose in phosphate buffer (10, 20, and 30%). The brain was extracted and cryoprotected in 30% sucrose. Sagittal sections (50  $\mu\text{m}$ ) were cut on a sliding microtome and mounted onto slides. Transduced cells were first localized by inspecting native fluorescence signals. Sections were then stained using primary antibodies against the reporter protein mCherry (Genetex GTX59788 RRID: AB\_10721869, 1:250) and against the pan-neuronal marker NeuN (millipore MAB377 RRID: AB\_2298772, 1:250), and using secondary antibodies (Invitrogen Molecular Probes): Alexa 568 (A10042 RRID: AB\_2534017, 1:400), Alexa 488 (A21206 RRID: AB\_141708 and custom, 1:400) and the nuclear stain DAPI (Invitrogen Molecular Probes D-21490, 1:5000) for visualization by epifluorescence microscopy.

**Neuron, Volume 110**

**Supplemental information**

**Deficits in decision-making induced  
by parietal cortex inactivation  
are compensated at two timescales**

**Danique Jeurissen, S. Shushruth, Yasmine El-Shamayleh, Gregory D. Horwitz, and Michael  
N. Shadlen**

**Monkey 1****Monkey 2****Monkey 3****Monkey 4**

**Figure S1. Stimulus configuration** (Related to Figure 1). The left and right choice-targets were positioned randomly on each trial using independent samples from the shaded regions of the visual field (uniform distribution over range of  $r, \theta$ ). For monkey 4, both choice targets were in either the upper or the lower hemifield. The area subtended by the random dot motion display (black circles; Monkeys 1 and 2) was consistent across trials/sessions and confined to the hemifield ipsilateral to the inactivated cortex. Eccentricities are in degrees visual angle.



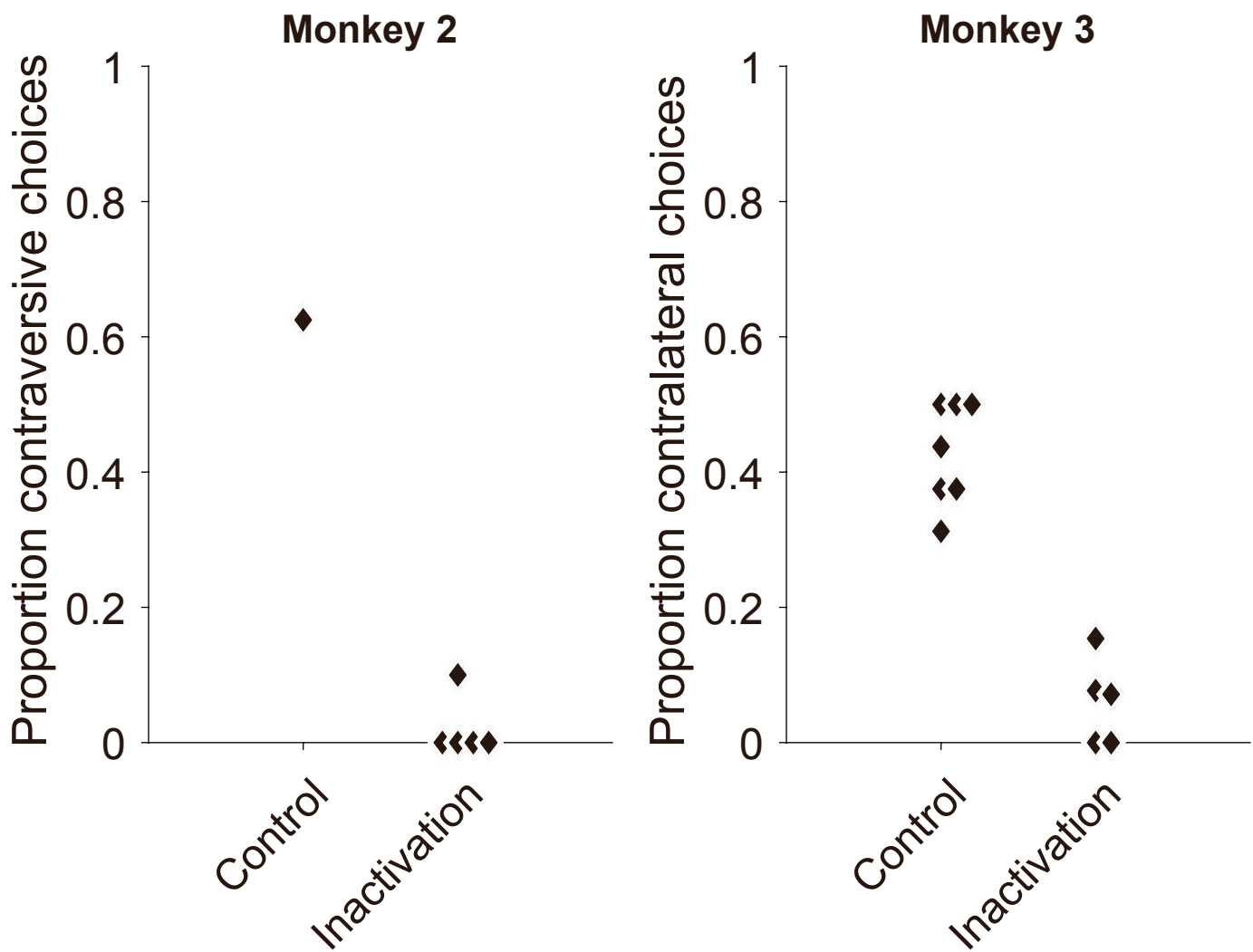


**Figure S2. Behavior on the side-preference task** (Related to Figure 2). After completion of the main experiment, Monkeys 2 and 3 were tested on a preference task intended to approximate a neurological double-simultaneous stimulation test for extinction. The experimenter presented desirable food items to the monkey's left and right side, equidistant from its mouth. The monkey indicated its preferred item by picking it with its tongue. The proportion of chosen items from the side contralateral to the inactivated cortex is shown. Points are data from one session. Points belonging to the same treatment group (control or muscimol inactivation) are displaced horizontally for visualization.

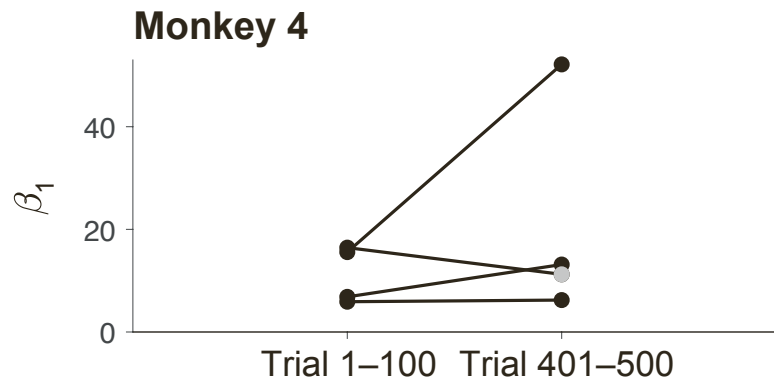
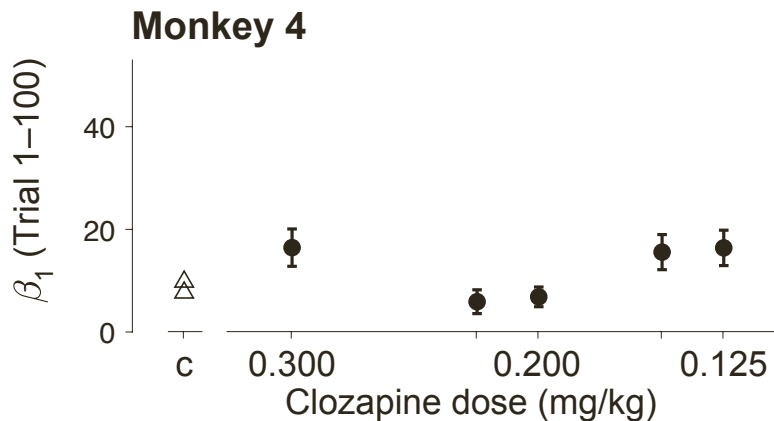
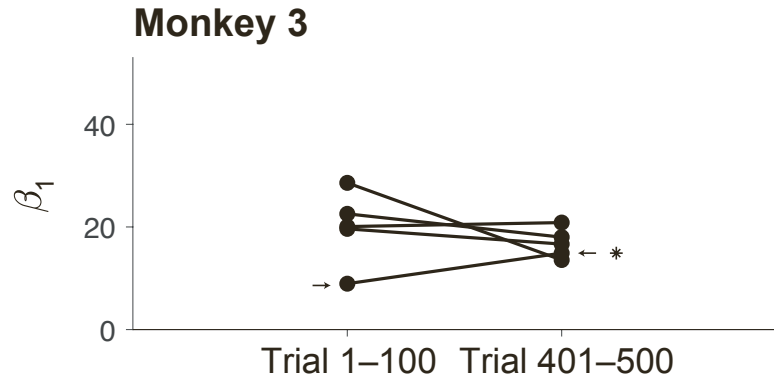
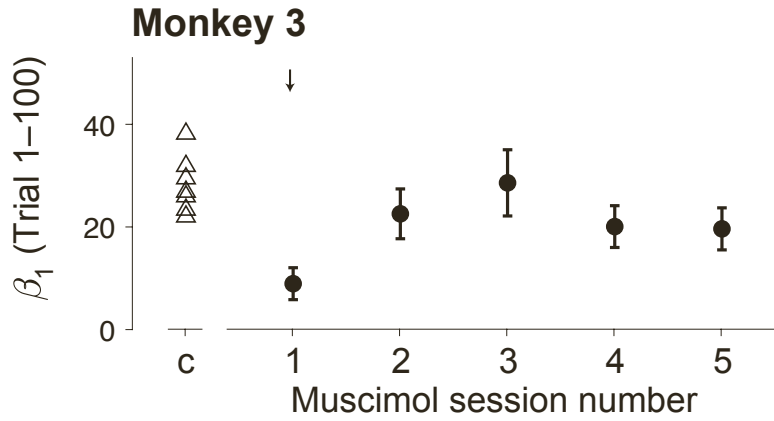
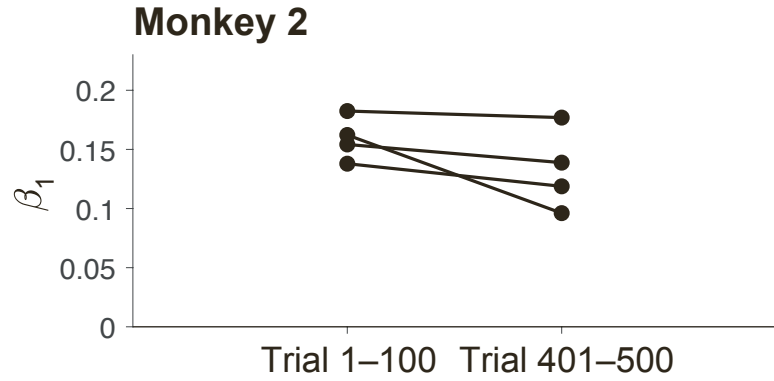
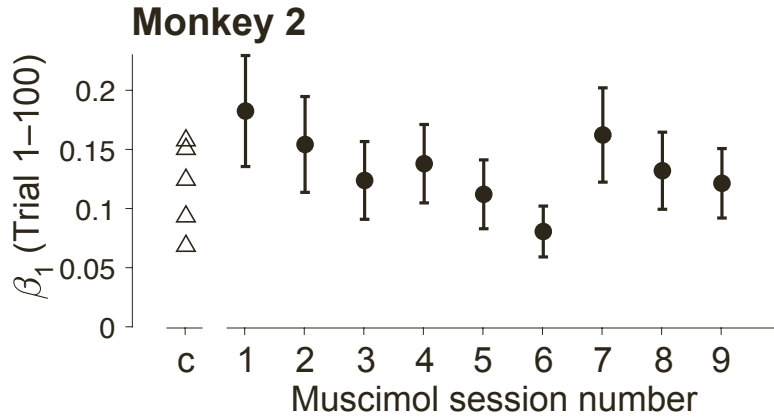
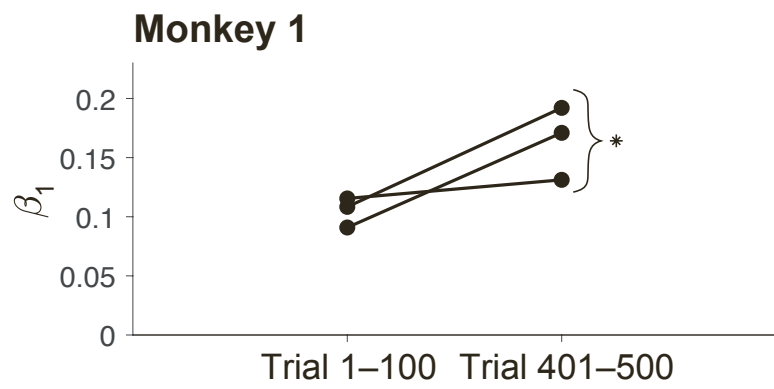
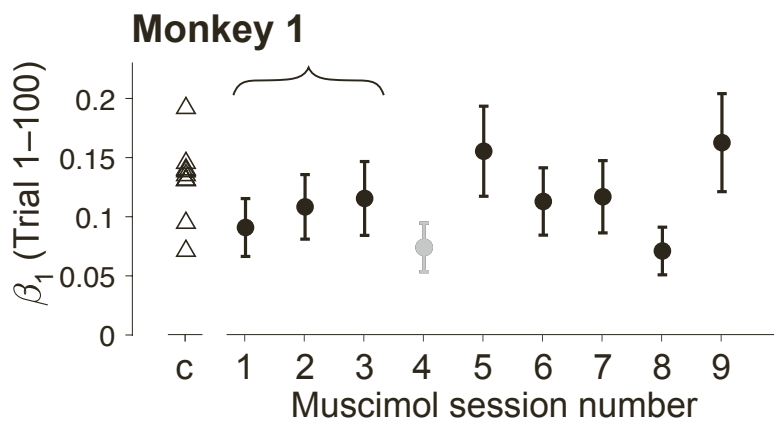


**Figure S3. Effect of inactivation on sensitivity** (Related to Figure 4). Data are from the same sessions as in Figure 4A–D. Here we show the values of the sensitivity parameter  $\beta_1$ . *Left column* shows sensitivity in the first 100 trials of each of the sessions. Inactivation led to reduced sensitivity in Monkey 1 (combined data from the first three sessions; curly brace) and in Monkey 3 (first session; arrow). *Right column* shows the comparison of sensitivity ( $\beta_1$ ) in the first 100 trials with trials 401–500 in the same session. All experiments with significant **bias** effect are shown (i.e., same experiments as in Figure 4C–D). These are the same experiments that exhibit reliable changes in sensitivity (Monkey 1) and they include the 1 experiment in Monkey 3 that revealed a change in sensitivity. Asterisks identify significant change in sensitivity between early and late trials, consistent with compensation. This applies to the grouped data for Monkey 1 and the first session for Monkey 3. Many sessions with significant changes in bias were not accompanied by reliable changes in sensitivity.

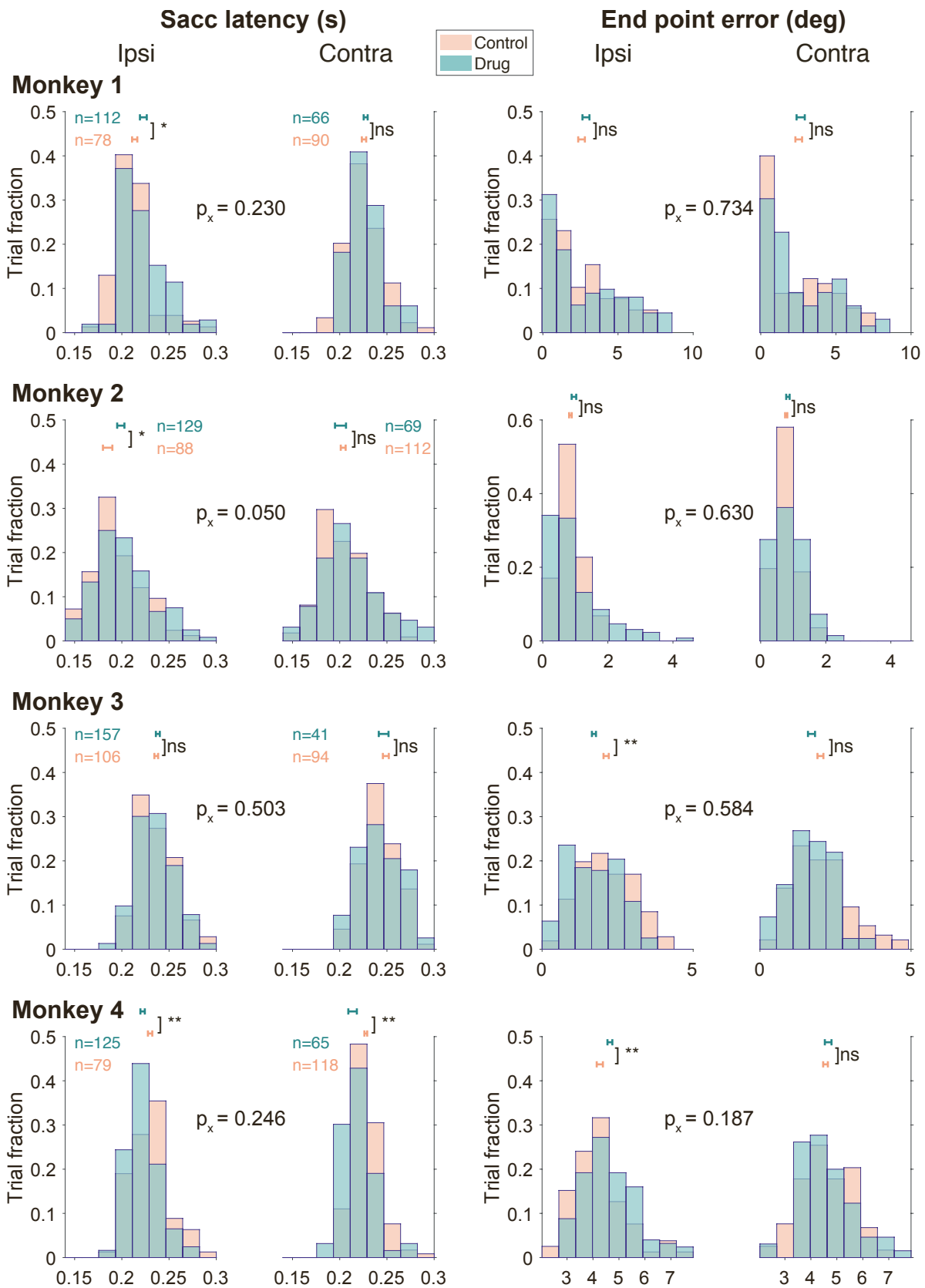


**Figure S4. Analysis of saccade metrics for the four monkeys** (Related to STAR Methods). Distributions of saccadic latency (left) and end-point error (right) are shown separately for the four monkeys (rows). Colors indicate inactivation (cyan) and control (pink) sessions. Each plot contains a pair of overlaid histograms for ipsiversive and contraversive saccades. The small horizontal error bars are  $\pm 1$  s.e.m. centered at the means. Asterisks indicate significant differences in the means for inactivation versus control (\*, \*\*:  $p < 0.05$ ,  $p < 0.01$ ; ns: not significant). P-values specified between the left and right histograms ( $p_x$ ) refer to the interaction between side and drug effects (Equation 10). An effect of inactivation on these saccade metrics was not detectable. Saccadic peak velocities (not shown) were similarly unaffected.

	pre vs. post			control vs post		
	value	SE	p	value	SE	p
Monkey 1	-0.77	0.34	0.02	-0.98	0.25	9e-05
Monkey 2	-1.08	0.40	0.01	-1.58	0.32	1e-06
Monkey 3	-2.31	0.50	4e-06	-1.90	0.42	6e-06
Monkey 4	-1.66	0.37	6e-06	-2.20	0.34	1e-10

**Table S1.  $\beta_2$  values, SE, and p values from Equation 5** (Related to STAR Methods and Figure 3).

	pre vs. post			control vs post		
	value	SE	p	value	SE	p
Monkey 1	-0.02	0.03	0.58	-0.03	0.03	0.32
Monkey 2	0.03	0.06	0.63	0.07	0.05	0.13
Monkey 3	-16.68	6.61	0.01	-17.77	3.87	4e-06
Monkey 4	-1.38	3.11	0.66	-2.79	2.78	0.32

**Table S2.  $\beta_3$  values, SE, and p values from Equation 5** (Related to STAR Methods and Figure 3).



Monkey	Task	Inactivation Method	Date	Session Type	Electrode Depth (µm)	Pipette Depth (µm)	Distance electrode to pipette (µm)	Injection Speed (µL/min)	Injected Volume	Drug Dose	Additional Info			
1	Motion	Pharmacology	20180109	Sham	-	-	-	-	-	-				
			20180121	Muscimol	8000	8500, 6700, 4900, 3100	x=1000, y=2000, z=500, D=2291	0.3	15 + 10 + 12 + 8 = 45µL	8µg/µL	1			
			20180626	Muscimol	6500	8000, 6200, 4400, 2600	x=1000, y=2000, z=1500, D=2693	0.3	3 + 6 + 6 + 4 = 19µL	8µg/µL				
			20180701	Muscimol	6500	8000, 6200, 4400, 2600	x=1000, y=2000, z=1500, D=2693	0.3	4 + 6 + 6 + 4 = 20µL	8µg/µL	%			
			20180705	Saline	6500	8000, 6200, 4400, 2600	x=1000, y=2000, z=1500, D=2693	0.3	4 + 6 + 6 + 4 = 20µL	-	%			
			20180803	Saline	7100	8000, 6200, 4400, 2600	x=1000, y=2000, z=900, D=2410	0.3	1 + 1 + 1 + 1 = 4µL	-				
			20180807	Muscimol	6500	8000, 6200, 4400, 2600	x=1000, y=2000, z=1500, D=2693	0.3	2 + 2 + 2 + 2 = 8µL	8µg/µL	#			
			20180814	Sham	-	-	-	-	-	-	-			
			20180815	Saline	6500	8000, 6200, 4400, 2600	x=1000, y=2000, z=1500, D=2693	0.3	4 + 6 + 6 + 4 = 20µL	-				
			20180816	Muscimol	6500	8000, 6200, 4400, 2600	x=1000, y=2000, z=1500, D=2693	0.3	4 + 6 + 6 + 4 = 20µL	8µg/µL				
			20180821	Sham	6900	-	-	-	-	-	-	*		
			20180822	Saline	6500	8000, 6200, 4400, 2600	x=1000, y=2000, z=1500, D=2693	0.3	4 + 6 + 6 + 4 = 20µL	-				
			20180823	Saline	6500	8000, 6200, 4400, 2600	x=1000, y=2000, z=1500, D=2693	0.3	4 + 6 + 6 + 4 = 20µL	-				
			20180824	Muscimol	6500	8000, 6200, 4400, 2600	x=1000, y=2000, z=1500, D=2693	0.3	4 + 6 + 6 + 4 = 20µL	8µg/µL	*			
			20180829	Saline	6500	8000, 6200, 4400, 2600	x=1000, y=2000, z=1500, D=2693	0.3	4 + 6 + 6 + 4 = 20µL	-				
			20180830	Muscimol	7150	8000, 6200, 4400, 2600	x=1000, y=2000, z=850, D=2392	0.3	4 + 6 + 6 + 4 = 20µL	8µg/µL				
			20180904	Muscimol	6500	8000, 6200, 4400, 2600	x=1000, y=2000, z=1500, D=2693	0.3	4 + 6 + 5.5 + 4.5 = 20µL	8µg/µL				
			20180914	Muscimol	6500	8000, 6200, 4400, 2600	x=1000, y=2000, z=1500, D=2693	0.3	4 + 6 + 6 + 4 = 20µL	8µg/µL				
			2	Motion	Pharmacology	20190808	Muscimol	3650	8000, 6200, 4400, 2600	x=2000, y=1000, z=4350, D=4891	0.4	4 + 6 + 6 + 4 = 20µL	8µg/µL	1
						20190814	Muscimol	3500	8000, 6200, 4400, 2600	x=2000, y=1000, z=4500, D=5025	0.4	4 + 6 + 6 + 4 = 20µL	8µg/µL	
20190829	Saline	3600				8000, 6200, 4400, 2600	x=2000, y=1000, z=4400, D=4936	0.4	5 + 5 + 6 + 4 = 20µL	-				
20190902	Muscimol	3500				8000, 6200, 4400, 2600	x=2000, y=1000, z=4500, D=5025	0.4	4 + 6 + 6 + 4 = 20µL	8µg/µL	N			
20190913	Sham	3600				-	-	-	-	-	-			
20191002	Sham	3600				-	-	-	-	-	-			
20191003	Muscimol	3600				8000, 6200, 4400, 2600	x=3000, y=1000, z=4400, D=5418	0.4	4 + 6 + 6 + 4 = 20µL	8µg/µL	N			
20191008	Sham	7000				-	-	-	-	-	-			
20191009	Muscimol	6800				8000, 6200, 4400, 2600	x=4000, y=1000, z=1200, D=4294	0.4	4 + 6 + 6 + 4 = 20µL	8µg/µL				
20191015	Muscimol	6600				8000, 6200, 4400, 2600	x=3000, y=1000, z=1400, D=3458	0.4	4 + 6 + 6 + 4 = 20µL	8µg/µL				
20191029	Sham	6150				-	-	-	-	-	-	N		
20191030	Muscimol	5400				8000, 6200, 4400, 2600	x=4000, y=1000, z=2600, D=4874	0.4	4 + 6 + 6 + 4 = 20µL	8µg/µL	N			
20191106	Muscimol	6500				8000, 6200, 4400, 2600	x=4000, y=1000, z=1500, D=4387	0.4	4 + 6 + 6 + 4 = 20µL	8µg/µL	N			
20191111	Muscimol	1700				8000, 6200, 4400, 2600	x=2000, y=1000, z=6300, D=6685	0.4	4 + 6 + 6 + 4 = 20µL	8µg/µL	N			
3	Time	Pharmacology				20200121	Sham	4000	-	-	-	-	-	N
			20200122	Sham	4000	-	-	-	-	-	N			
			20200128	Sham	4100	-	-	-	-	-	N			
			20200207	Muscimol	8000	8500, 6700, 4900, 3100	x=2000, y=0, z=500, D=2062	0.4	4 + 6 + 6 + 4 = 20µL	8µg/µL	N, 1			
			20200213	Muscimol	6850	8500, 6700, 4900, 3100	x=2000, y=0, z=1650, D=2593	0.4	4 + 6 + 6 + 4 = 20µL	8µg/µL	N			
			20200218	Sham	6500	-	-	-	-	-	-	N		
			20200221	Sham	4800	-	-	-	-	-	-	N		
			20200225	Muscimol	5200	8500, 6700, 4900, 3100	x=3000, y=0, z=3300, D=4460	0.4	4 + 6 + 6 + 4 = 20µL	8µg/µL	N			
			20200303	Sham	3000	-	-	-	-	-	-	N		
			20200304	Muscimol	4500	8500, 6700, 4900, 3100	x=4000, y=1000, z=4000, D=5745	0.4	4 + 6 + 6 + 4 = 20µL	8µg/µL	N			
			20200310	Sham	4100	-	-	-	-	-	-	N		
			20200311	Muscimol	4500	8500, 6700, 4900, 3100	x=4000, y=1000, z=4000, D=5745	0.4	4 + 6 + 6 + 4 = 20µL	8µg/µL	I, N			
			4	Time	Chemo-genetics	20171121	Viral injection	13 locations, each spaced 500µm apart, between 9800 and 3800	13 locations, each spaced 500µm apart, between 9000 and 3000	800	0.1	13 injections of 0.5µL each. Total volume: 6.5 µL	-	vi
20171122	Viral injection	14 locations, each spaced 500µm apart, between 9700 and 3200				14 locations, each spaced 500µm apart, between 9000 and 2500	700	0.1	14 injections of 0.5µL each. Total volume: 7µL	-	vi			
20180522	Clozapine	9000				-	-	-	-	0.125 mg/kg	v			
20180604	Clozapine	7000				-	-	-	-	0.300 mg/kg	v, *, 1			
20180608	Clozapine	-				-	-	-	-	0.150 mg/kg				
20180727	Saline	-				-	-	-	-	-				
20180731	Clozapine	-				-	-	-	-	0.200 mg/kg				
20180807	Saline	-				-	-	-	-	-				
20190809	Clozapine	-				-	-	-	-	0.225 mg/kg				

**Table S3. List of all experimental sessions** (Related to STAR Methods). Sessions are sorted by date for each monkey. The electrode and pipette depths are in micrometers below the dura. Electrode depth was constant throughout the session and we list the depth of either the tip of the electrode (single channel) or deepest electrode (24-channel V-probe). For muscimol infusion, the pipette was placed at four different depths. The injected volume is reported for each depth. For the muscimol infusion experiments, the distance between the recording electrode and the deepest pipette location is reported (i.e., first injection site).

**Symbols and abbreviations:**

Motion: Motion direction task.

Time: Temporal order task.

\*: Monkey completed < 50 trials post injection.

%: Strongest motion strength (coherence +/-51.2%) was not used in this session.

#: Low-volume muscimol injection session.

I: Last session in Monkey 3. Further sessions were not possible due to the health and safety restrictions related to the COVID-19 pandemic.

vi: Viral vector injection session.

v: Sessions with V-probe recordings. Data shown in Figure 2D.

N: Collected data on side-preference task.

1: First (high-dose) session. Data shown in Figure 3.